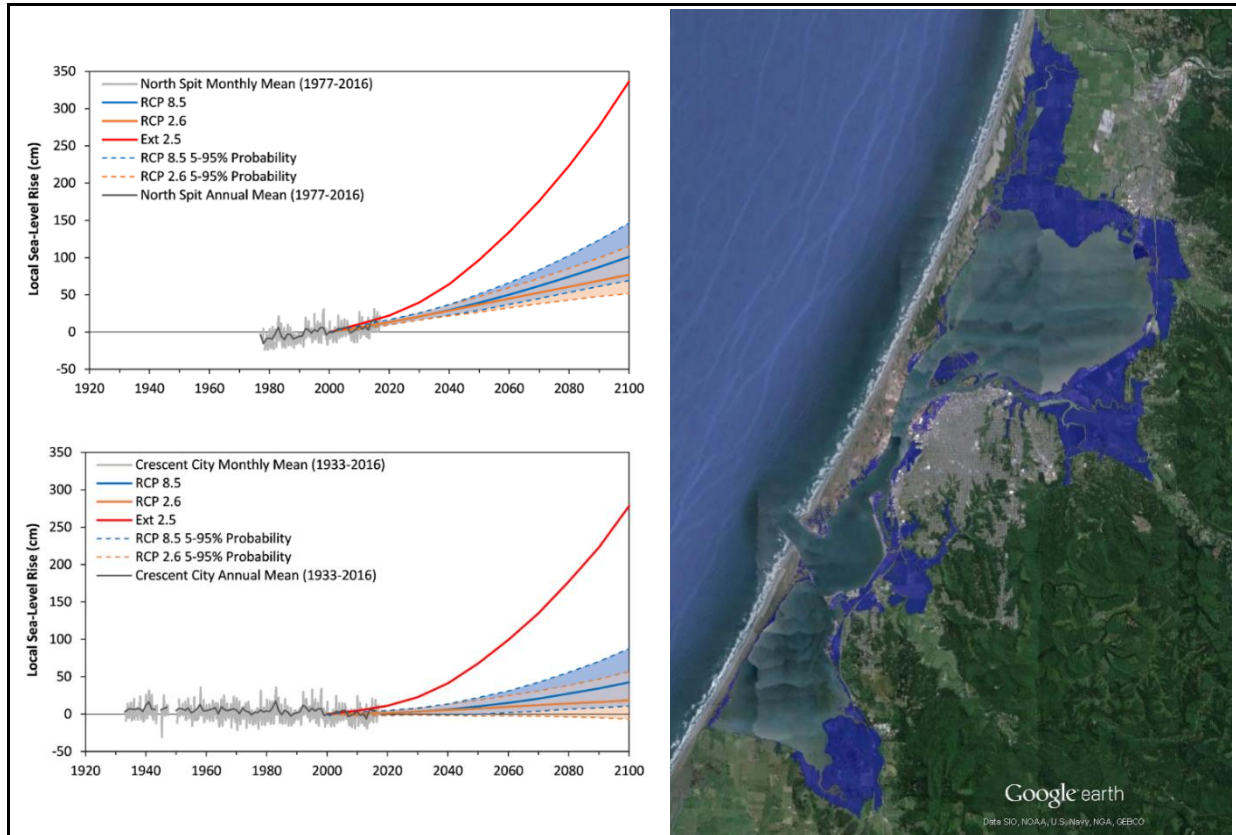


Sea-Level Rise in the Humboldt Bay Region

Update 1: March 2018



Prepared by

Jeffrey K. Anderson

Northern Hydrology & Engineering

P.O. Box 2515

McKinleyville, CA 95519



Preparation of this document was partially funded by the City of Arcata.

Sea-Level Rise in the Humboldt Bay Region

Sea-level rise is one of the most evident and problematic consequences of global climate change. As the earth's climate warms, sea levels increase primarily from thermal expansion of a warmer ocean and melting land ice (NRC, 2012). In California, sea-level rise will threaten and directly affect vulnerable coastal ecosystems, bays and estuaries, coastal communities and infrastructure due to increased flooding, gradual inundation, and erosion of the coastal shorelines, cliffs, bluffs and dunes (Russell and Griggs, 2012). If sea level continues to rise at present rates, identified impacts could take decades or longer to occur. However, a troublesome aspect of climate change and the rapid warming of the earth's atmosphere and ocean is the potential for sea-level rise to accelerate to high rates over a short period of time, in which case the identified impacts could happen within a much shorter period (years to decades). Although there is uncertainty in the timing of sea-level rise and future impacts, society still needs to plan for, and adapt to higher sea levels.

The coasts of Humboldt and Del Norte Counties are experiencing the combined effects of global sea-level rise, regional sea-level height variability from seasonal to multidecadal ocean-atmosphere circulation dynamics (e.g. El Niño Southern Oscillation (ENSO)), and relatively large tectonic vertical land motions associated with the Cascadia subduction zone (CSZ) (Figure 1). These large tectonic motions along the southern CSZ create the highly variable and opposing sea-level trends observed between Humboldt Bay and Crescent City. Recent estimates of land subsidence by Patton et al. (2017) indicate that Humboldt Bay has the highest local sea-level rise rate in California, approximately two to three times higher than the long-term global rate. In contrast, the land in Crescent City (109 km north) is uplifting faster than long-term global sea level rise, which causes a negative or decreasing local sea-level rise rate.

Overview and Purpose

The purpose of this chapter is to provide an overview of global and regional sea-level rise, with an emphasis on physical processes locally affecting sea levels in the Humboldt Bay region, and provides an update to Chapter 2 of the Humboldt Bay: Sea Level Rise, Hydrodynamic Modeling, and Inundation Vulnerability Mapping report (NHE, 2015a). This overview relies on the past climate and sea-level change literature (e.g. NRC, 2012; IPCC, 2013; Church et al., 2013), the more recent sea-level science literature (e.g. Kopp et al., 2014; Kopp et al., 2015; Hall et al., 2016; Sweet et al., 2017; Griggs et al., 2017), the scientific and technical literature specific to the U.S. Pacific Northwest (PNW) coast (e.g. Burgette et al., 2009; Komar et al, 2011), and literature specific to the Humboldt Bay region (e.g. NHE, 2015a; Patton et al., 2017).

In 2017, the Ocean Protection Council (OPC) Science Advisory Team released its updated sea-level rise science report, titled *Rising Seas in California: An Update on Sea-Level Rise Science* (Griggs et al., 2017). The OPC report provides an update on the current state of sea-level rise science, along with a synthesis of the current scientific understanding of potential Greenland and

Antarctic ice sheet loss and implications for sea-level rise projections in California. The OPC report also provided probabilistic sea-level rise projections at three locations along the California coast (Crescent City, San Francisco, and La Jolla) based on the approach of Kopp et al. (2014).

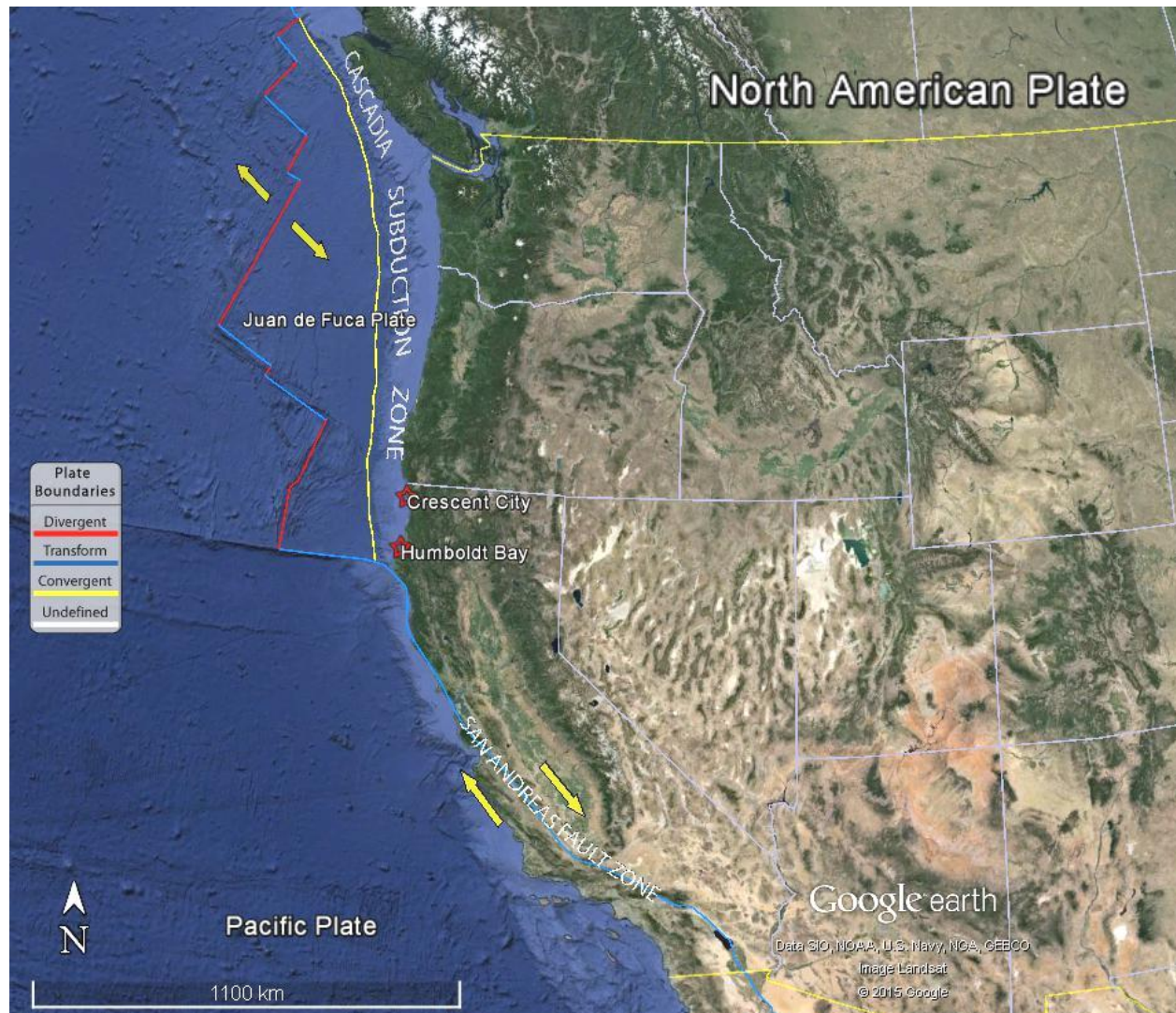


Figure 1. Tectonic plate boundaries along the U.S. west coast, and the location of Humboldt Bay and Crescent City relative to the Cascadia subduction zone. Tectonic boundary data downloaded from <http://earthquake.usgs.gov/learn/kml.php>.

The OPC (2017) report did not address local issues affecting sea-level rise in the Humboldt Bay region, or provide projections applicable for the region. A key purpose of this chapter is to provide probabilistic sea-level rise projections for the Humboldt Bay region based on the work of Kopp et al. (2014) and the local estimates of vertical land motion by Patton et al. (2017). The updated overview and probabilistic projections provides decision makers the most up-to-date and

locally relevant information to support planning and developing adaptation strategies for sea-level rise in the Humboldt Bay region.

Global Climate System Change

In 2013, the IPCC completed its Fifth Assessment Report (AR5). The AR5 states that continued emissions of greenhouse gases (carbon dioxide, methane, and nitrous oxide) will cause changes in all components of the global climate system, affecting temperature and precipitation patterns, ocean temperatures and chemistry, ocean-climate variability, and sea-level rise. The AR5 reports (95% confidence) that human activity is the dominant cause of the observed global climate system warming since the mid-20th century (Figure 2), with the last three decades being successively warmer than any preceding decade since 1850. Furthermore, atmospheric concentrations of greenhouse gases have increased to levels unprecedented in at least the last 800,000 years. Carbon dioxide concentrations have increased by 40% since pre-industrial times, with the ocean absorbing about 30% of the emitted anthropogenic carbon dioxide (Figure 3), causing ocean acidification (IPCC, 2013). The AR5 concluded that limiting climate change will require substantial and sustained reductions of greenhouse gas emissions.

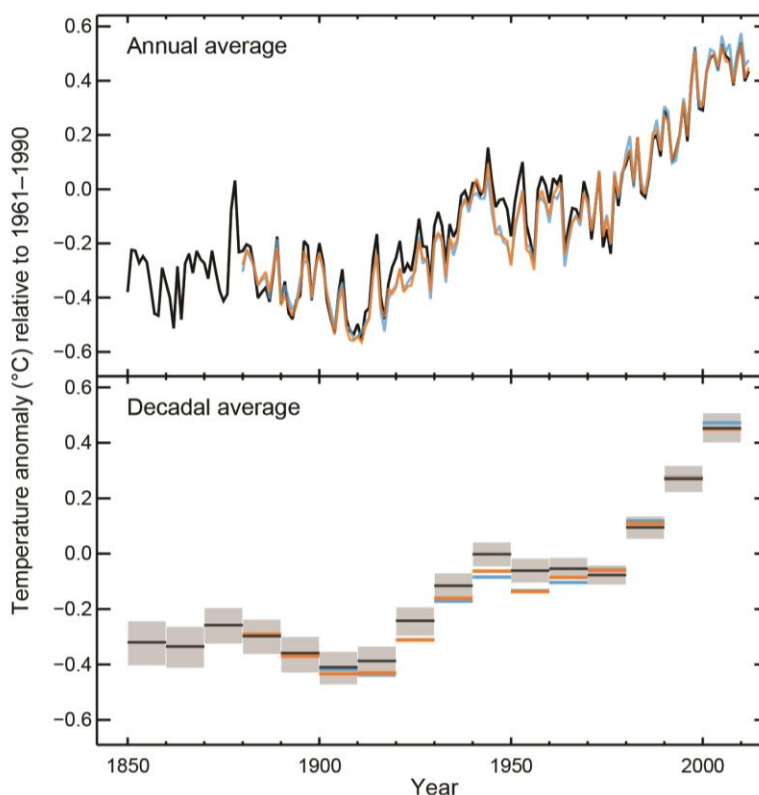


Figure 2. Observed 1850 to 2012 global mean combined land and ocean surface temperature anomalies (relative to the mean of 1961-1990) from three datasets. Top panel is the annual mean values, and bottom panel are the decadal mean values with uncertainty for one dataset (black). (Figure from IPCC, 2013)

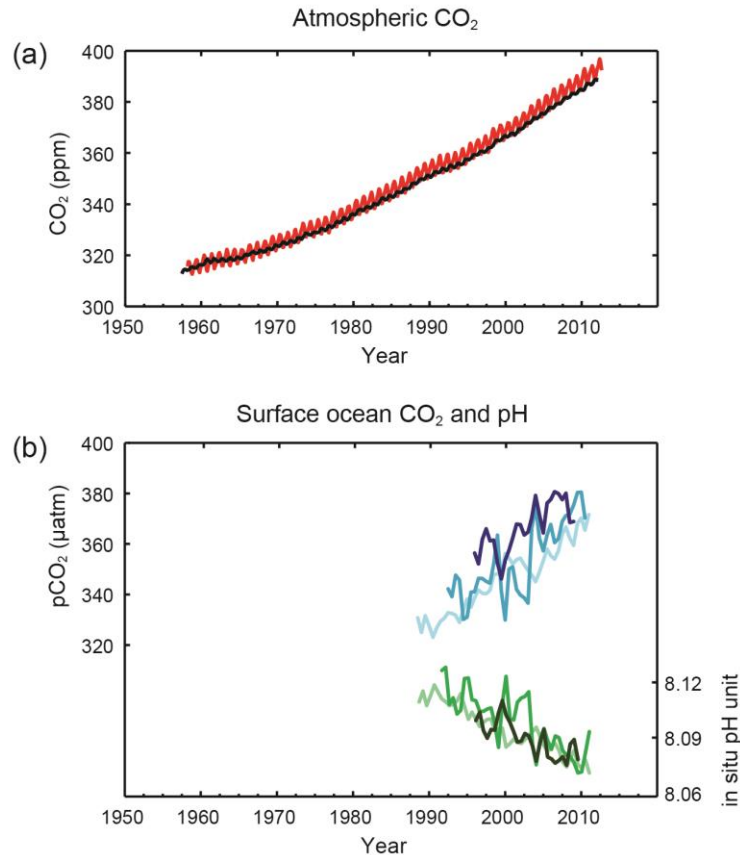


Figure 3. (a) Observed atmospheric carbon dioxide (CO₂) concentrations for Mauna Loa (red line) and South Pole (black line) since 1958. (b) Ocean surface observed partial pressure of dissolved CO₂ (blue lines), and in situ pH (green lines) which is an indicator of ocean acidification. Measurements from Atlantic Ocean (dark blue and dark green, and blue and green) and Pacific Ocean (light blue and light green). (Figure from IPCC, 2013)

Past and Present Sea-Level Rise

This section provides an overview of sea-level change associated with global mean sea-level (GMSL) rise, regional sea-level (ReSL) rise, and local sea-level (LSL) rise.

Global Mean Sea-Level

Global mean sea levels have been increasing since the last ice age about 20,000 years ago (Russell and Griggs, 2012; Kominz, 2001), although at relatively low rates (~ 0.1 mm/yr) over the last two millennia (NRC, 2012). There is high confidence, based on proxy records (e.g. salt marsh sediments) and instrumental sea-level data, that GMSL rise increased in the late 19th to early 20th century from relatively low rates over the previous two millennia to higher rates today (Church et al., 2013). The dominant contributors to GMSL rise over the last century are atmospheric and ocean warming, which increases ocean volume through ocean thermal expansion, and increases ocean mass from melting land ice and, to a lesser extent, land water storage and groundwater extraction (Rhein et al., 2013; Church et al., 2013).

Analysis of global tide gauge records dating back to the 1880s (Church and White, 2011), and the more recent satellite altimetry observations of sea surface change from 1993 to present (Beckley et al., 2010) clearly indicate that GMSL rise rates have increased since 1993 (Figure 4, Table 1). The tide gauge reconstructions by Church and White (2011) indicate that the rate of GMSL rise between 1901 to 1990 was 1.5 ± 0.2 mm/yr, and from 1901 and 2010 was 1.7 ± 0.2 mm/yr. The rate of GMSL rise measured by satellite altimetry from 1993 to 2016 is 3.4 ± 0.4 mm/yr (<https://sealevel.nasa.gov>, data accessed in September 2017), which is two times or more the tide gauge rates listed above. Recently, Hay et al. (2015) reanalyzed the tide gauge data using probabilistic techniques and estimated a GMSL rise rate of 1.2 ± 0.2 mm/yr from 1901 to 1990, which is lower than the Church and White (2011) estimate for the same period. This indicates that the increase in GMSL rates from 1993 to 2016 (altimetry rate of 3.4 ± 0.4 mm/yr) over the 1901 to 1990 rates is greater than previously thought (Hay et al., 2015). Although these methods result in different estimates of the rate of GMSL rise, they all indicate the same overall pattern of increased rates in recent decades.

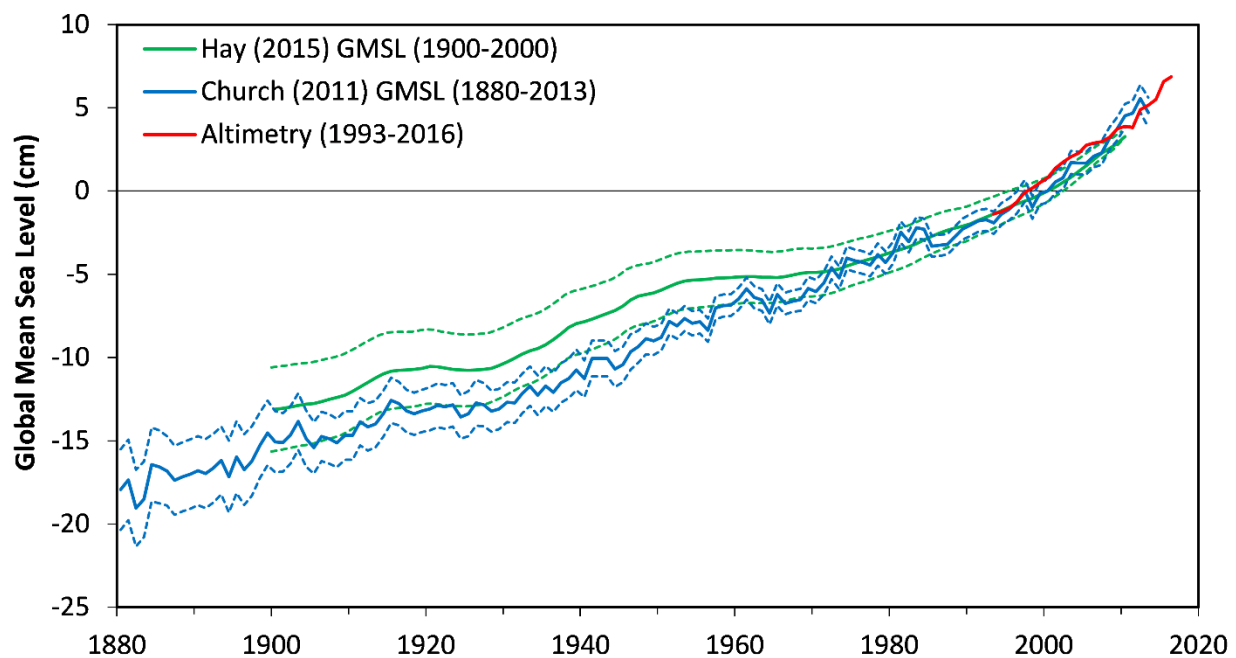


Figure 4. Yearly average reconstructed GMSL (blue line) for 1880 to 2013 of Church and White (2011) with one standard deviation uncertainty bounds (blue dashed line), data downloaded from <http://www.cmar.csiro.au>. Reconstructed GMSL (green line) for 1901 to 2010 of Hay et al. (2015) with one standard deviation uncertainty bounds (green dashed line), data downloaded with publication. Satellite altimeter data for 1993 to 2016 of Beckley et al. (2010), data downloaded at: <https://sealevel.nasa.gov>. All data relative to year 2000 baseline.

Table 1. Estimated GMSL rise rates and uncertainty range (90% confidence interval) for different time periods. Data from Church and White (2011), Hay et al. (2015), Rhein et al. (2013) and Beckley et al. (2010).

| Time Period | GMSL Rise Rate and Uncertainty (mm/yr) | Source |
|--------------|--|--|
| 1901 to 1990 | 1.5 [1.3 to 1.7] | Tide gauge reconstruction (Church and White, 2011) |
| 1901 to 1990 | 1.2 [1.0 to 1.4] | Tide gauge reconstruction (Hay et al., 2015) |
| 1901 to 2010 | 1.7 [1.5 to 1.9] | Tide gauge reconstruction (Church and White, 2011) |
| 1993 to 2016 | 3.4 [3.0 to 3.8] | Satellite altimetry data (Beckley et al., 2017) |

Regional Sea-Level Rise

As mentioned above, the dominant drivers to GMSL rise are thermal expansion of the ocean, increases in ocean mass from melting land ice, and to a lesser extent, changes in land water storage. However, the spatial or ReSL rise can differ from GMSL rise due to a range of factors such as ocean dynamics, climate variability, and sea-level fingerprints (Cayan et al., 2008; NRC, 2012; Church et al., 2013; Kopp et al., 2014; Kopp et al., 2015). Figure 5 shows the monthly mean LSL rise trends at three NOAA long-term (greater than 100-years) tide gauges located on relatively tectonically stable ground (Cayan et al., 2008; Burgette et al., 2009; Bromirski et al., 2011). The three sea-level rise trends are consistent, ranging from 1.94 to 2.15 mm/yr, with the average (2.0 mm/yr) representing an estimate of ReSL rise along the U.S. west coast. This rate is 18% greater than the 1901 to 2010 GMSL trend of 1.7 mm/yr (Table 1), implying that over the instrument period ReSL rise along the U.S. west coast has been greater than GMSL rise. The dominant factors affecting ReSL change along the U.S. west coast are summarized below.

Ocean Dynamics and Climate Variability. Non-uniform sea-level changes arise from ocean dynamics, circulation, heat content, and salinity differences due to freshwater (mass) inputs from ice loss, regional wind and current patterns, and coupled ocean-atmosphere processes from natural climate variability. The most important climate processes along the U.S. west coast affecting sea-level change are the seasonal cycle, ENSO, and the Pacific Decadal Oscillation (PDO) (Komar et al., 2011; Bromirski et al., 2011; NRC, 2012).

Seasonal coastal current and wind patterns (e.g. upwelling) produce variations in sea levels, known as the average seasonal cycle, due to ocean temperature and density changes (Zervas, 2009; Komar et al., 2011). ENSO causes seasonal to interannual timescale climate variability with more active winter storm periods and higher sea levels during the warmer El Niño phase, and lower levels during the cooler La Niña phase (Figure 6). The PDO is described as an interdecadal ENSO like pattern of climate variability in the Pacific Ocean with warm and cool phases (Figure 6) that shift on interdecadal timescales of about 20 to 30 years (Zhang et al., 1997; Mantua et al., 1997).

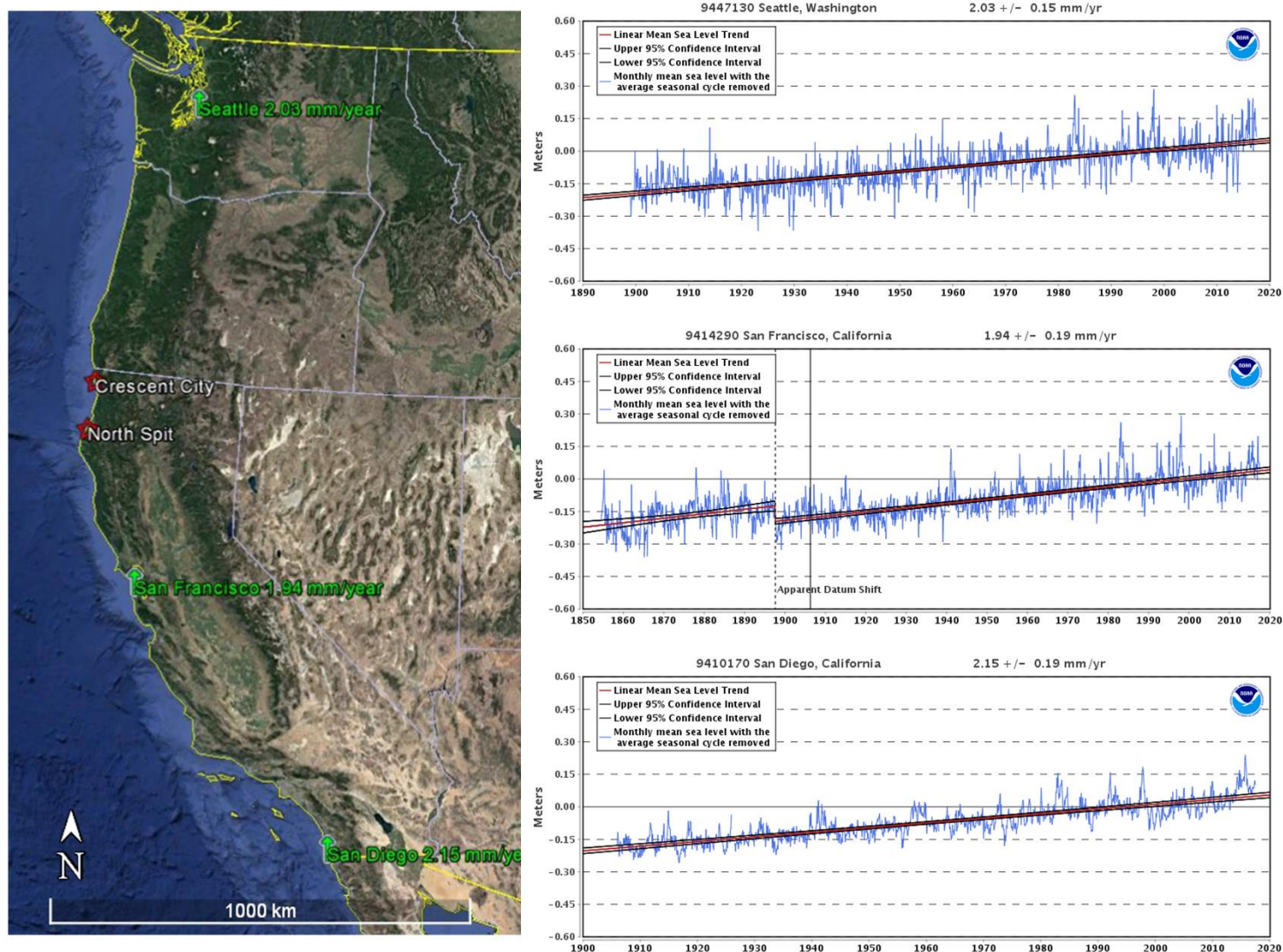


Figure 5. Observed monthly ReSL rise trends for NOAA tide gauge records for Seattle, San Francisco and San Diego. These tide gauge sites are located on relatively tectonically stable ground. Data and figures accessed on October 2017 at <http://tidesandcurrents.noaa.gov>.

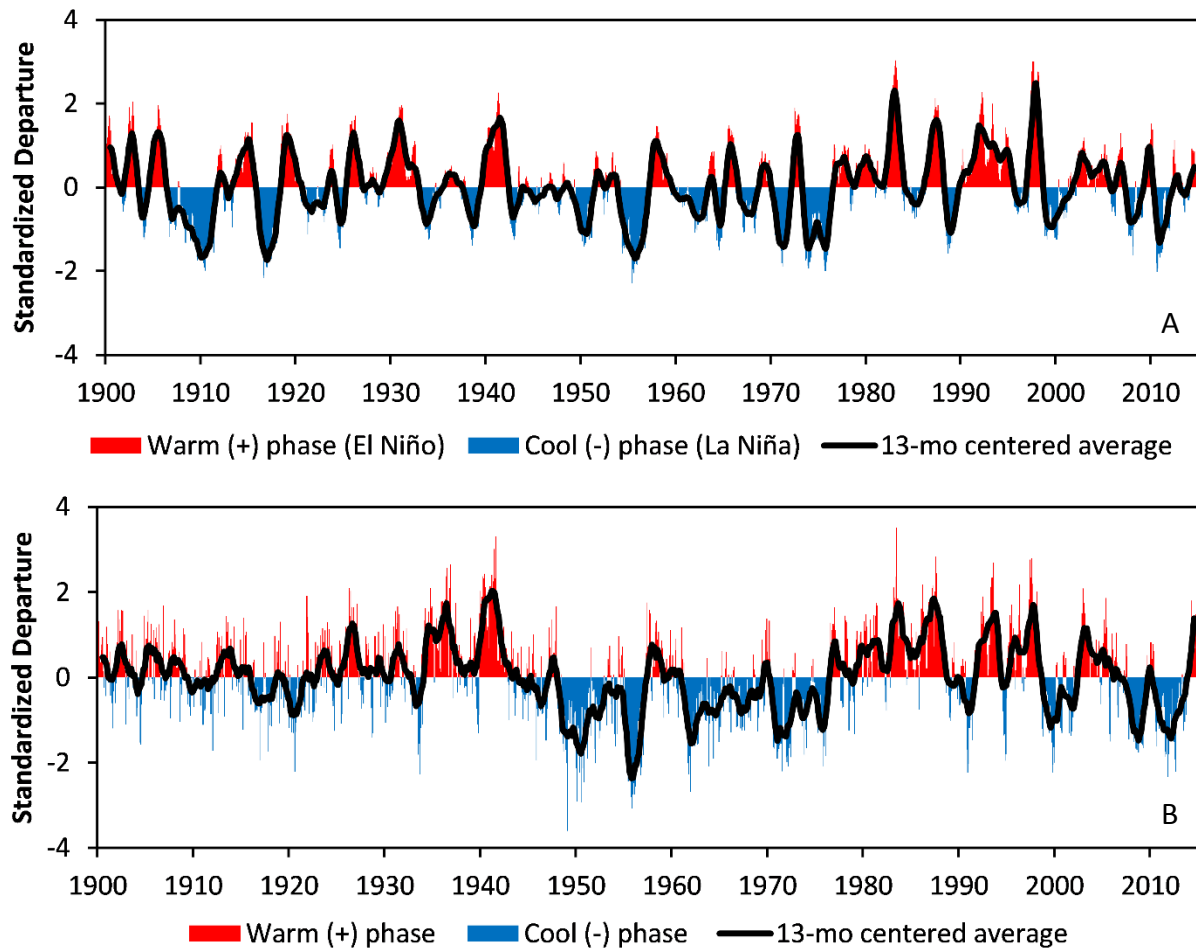


Figure 6. (A) Multivariate ENSO index (MEI), and (B) Pacific Decadal Oscillation (PDO) index from 1900 to March 2015. The black lines are 13-month centered average values. MEI index based on MEI.ext data from 1900 to 1949 (Wolter and Timlin, 2011), and MEI data from 1950 to March 2015 (Wolter and Timlin, 1993, 1998); MEI data downloaded from <http://www.esrl.noaa.gov/psd/enso>. PDO index data from 1900 to March 2015 (Mantua et al., 1997); PDO data downloaded from <http://research.jisao.washington.edu/pdo>. Refer to sources and links for details on how the MEI and PDO indexes were computed.

Bromirski et al. (2011) attributes suppression of the ReSL trend along the U.S. west coast since the 1980s (Figure 5) to changes in the wind stress curl associated with the PDO regime shift in the mid-1970s (Figure 6). Recently, Hamlington et al. (2016) noted an apparent PDO shift resulting in higher sea levels along the U.S. west coast over the last few years that could persist, leading to higher rates of sea-level rise, similar to the higher rates in the observational record.

Sea-Level Fingerprints. Changes to the Earth’s gravitational and deformational response to mass redistribution between the ocean and glaciers, ice caps and ice sheets (cryosphere) is known as sea-level or static-equilibrium fingerprints. As land ice melts, water enters the ocean raising

GMSL; however, a reduced gravitational pull on the ocean water also results from the decrease in ice mass. The overall net effect of these fingerprints is that ReSL will drop near the melting ice masses, and increase proportional to the distance from the ice masses.

Vertical land motion. Vertical land motion (VLM) is associated with tectonics, sediment compaction and/or subsidence, and glacial isostatic adjustment (GIA). GIA is the response of the Earth's surface to the retreat of the ice sheets during the last ice age. Regional and local VLM, such as tectonic land-level changes, can be much larger than those associated with GIA models (Zervas, 2009). Along the U.S. west coast, and in particular the CSZ, researchers have documented interseismic tectonic land-level rates from plate locking that are an order of magnitude greater than the global GIA rate (Mitchell et al., 1994; Burgette et al., 2009). Along the PNW coast, the tectonic land-level changes associated with the CSZ strongly affect regional and local sea-level changes (Komar, 2011).

Regional Sea-Level Rise along the Pacific North West Coast and Humboldt Bay Region

To infer VLM associated with tectonic uplift rates from LSL change at six NOAA tide gauge sites located between Crescent City, CA and Astoria, OR, Burgette et al. (2009) determined an average sea-level rise rate of 2.28 ± 0.20 mm/yr that represents an approximate 20th century ReSL rise rate for the PNW coast along the CSZ. As noted by Burgette et al. (2009), the 2.28 mm/yr ReSL rise rate compared well to the 1950 to 2000 GMSL reconstruction of Church and White (2006), which had trend slopes for grid points offshore of the CSZ of 2.2 ± 0.30 mm/yr. Komar et al. (2011) further assessed the 2.28 mm/yr ReSL rate by comparing LSL rates for the six CSZ tide gauge records to the benchmark and Pacific Northwest Geodetic Array Global Positioning System (GPS) data, and concluded that the rate is reasonable for the PNW coast. Finally, the NRC (2012) study determined an adjusted (for VLM and atmospheric pressure) sea level rise rate of 2.30 mm/yr for the Seattle tide gauge for the 1900 to 2008 period, which is also consistent with the 2.28 mm/yr ReSL rise rate.

The 2.28 mm/yr ReSL rise rate is 0.58 mm/yr greater (34% increase) than the 1901 to 2010 GMSL rate of 1.7 mm/yr (Table 1). This implies that natural climate variability (ENSO and PDO), ocean dynamic processes, and gravitational mass redistribution have produced a greater ReSL rise rate for the PNW coast relative to the GMSL rate for the same general period. The Burgette et al. (2009) rate of 2.28 mm/yr has been used by local researchers (e.g. NHE, 2015a; Patton et al., 2017) to represent historic ReSL rise rates for the Humboldt Bay region.

Past and Present Local Sea-Level Rise

Tide gauges measure local sea-level (LSL) change, which is the combined effects of sea-level change and VLM. The measured LSL change includes the same processes affecting ReSL patterns, and other short-term local processes such as wind waves, tides and hydrodynamic effects. As noted by Zervas (2009), VLM is responsible for most of the differences in LSL trends between regional tide observations. For example, although the Crescent City and North Spit tide

gauges are only separated by 109 km (~68 mi), the LSL trends for these gauges are in opposing directions (Figure 7).

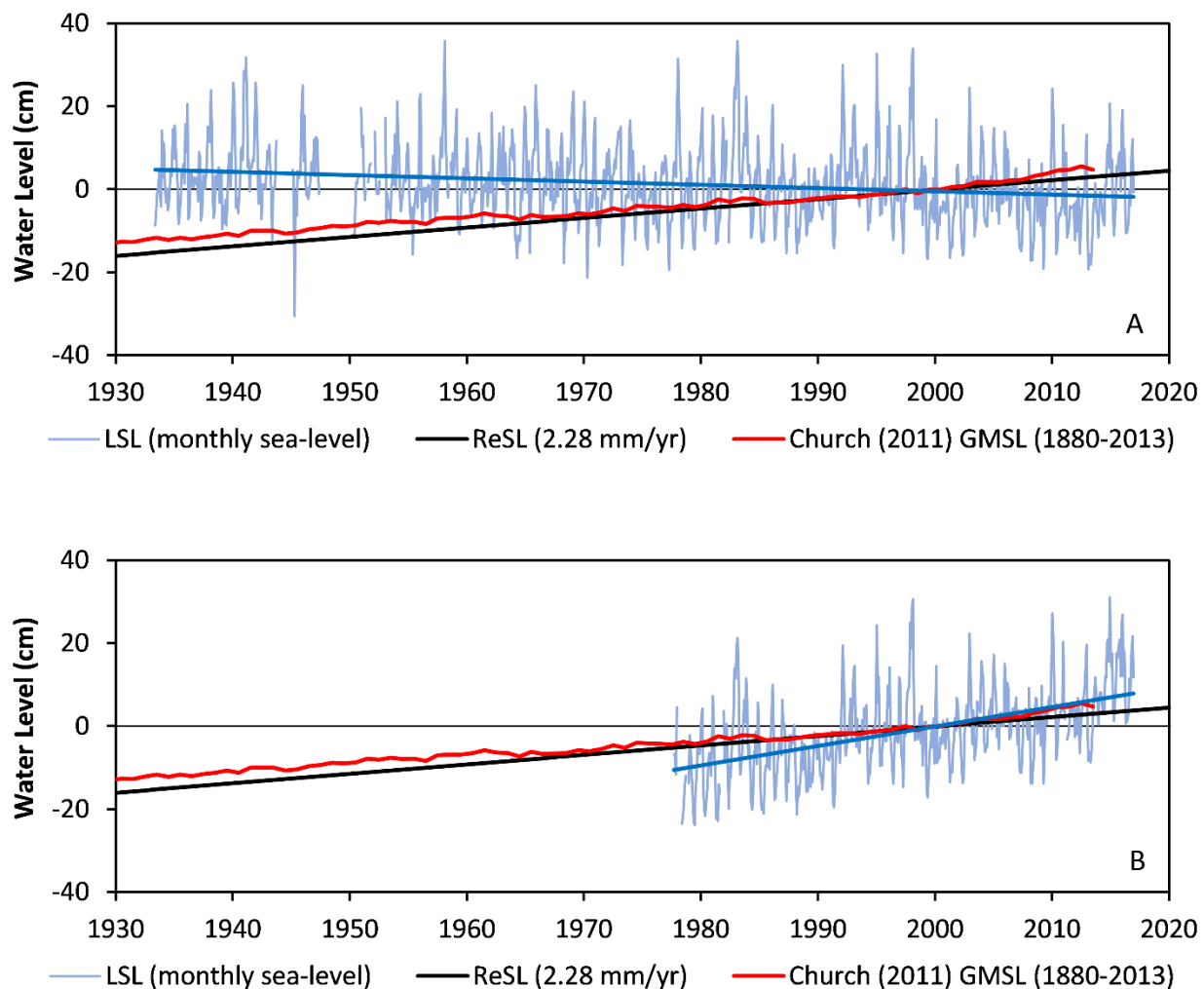


Figure 7. (A) LSL change for Crescent City tide gauge (1933 to 2016). (B) LSL rise for Humboldt Bay North Spit tide gauge (1977 to 2016). LSL changes (light blue lines) are monthly mean values, LSL trends (dark blue lines) are the linear regression on the monthly values, ReSL rise trend (black line) is the Burgette et al. (2009) ReSL rate of 2.28 mm/yr., GMSL rise trend (red line) is the Church and White (2011) reconstruction. All data relative to year 2000 baseline.

The downward LSL trend at Crescent City indicates this section of coast is emerging, with an uplift rate greater than the current GMSL and ReSL rise rates. In contrast, the North Spit LSL trend is greater than the GMSL or ReSL rates, indicating that Humboldt Bay is submergent, and in fact, has the highest LSL rise rate of any tide gauge in California. The relatively large oscillations in monthly LSL values around the trend line are due to short-term weather variability (e.g. storms), natural climate variability (e.g. ENSO and PDO), and the average seasonal cycle.

Local Sea-Level Rise and Vertical Land Motion Rates in the Humboldt Bay Region

The LSL rise rate at North Spit tide gauge is greater than both the GMSL and ReSL rise rates due to land subsidence in and around Humboldt Bay. To better understand how tectonic land motion affects LSL rates in Humboldt Bay, Cascadia Geosciences and partners received funding from the U.S. Fish & Wildlife Service (study plan at <http://www.hbv.cascadiageo.org>) to utilize tide gauge observations, benchmark level surveys, and GPS data to evaluate tectonic VLM and LSL rates in Humboldt Bay. The tide gauge analysis evaluated water level observations at the NOAA Crescent City tide gauge, and five NOAA tide gauge sites in Humboldt Bay, which include North Spit and four historic gauges located at Mad River Slough, Samoa, Fields Landing, and Hookton Slough (Figure 1, Figure 8).

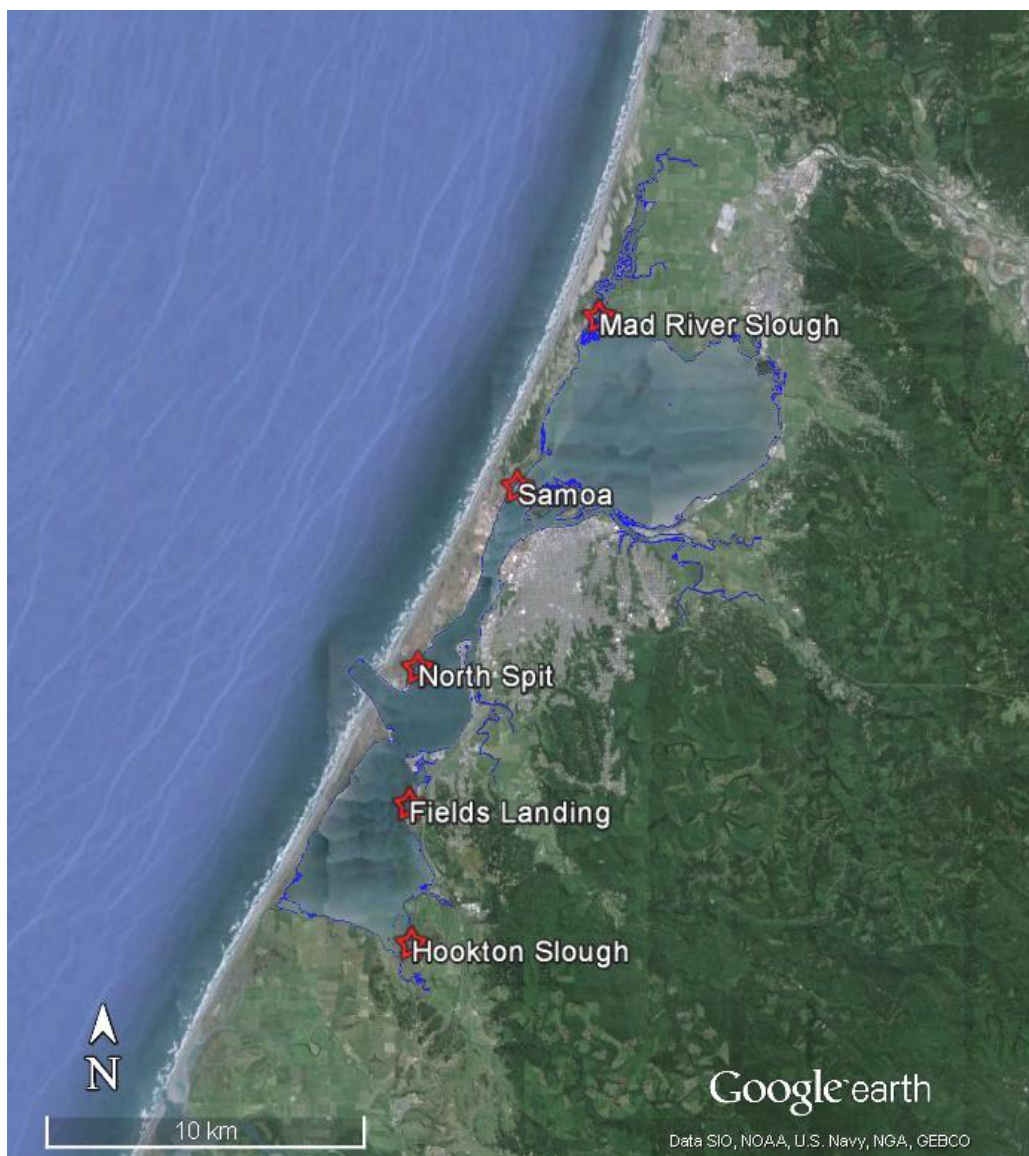


Figure 8. Five NOAA tide gauge locations in Humboldt Bay, and mean high water edge (blue line).

The tide gauge analysis relied on the long-term Crescent City (~84 years) and North Spit (40 years) tide gauges, and the general approach of Mitchell et al. (1994) and Burgette et al. (2009) to determine VLM and LSL rates at the other Humboldt Bay gauges, which all have record lengths less than 30 years and are considered too short to directly determine rates (Zervas, 2009). The analysis also relied on the 20th century ReSL rise rate (2.28 mm/yr) of Burgette et al. (2009).

Recently, NHE (in progress) updated the original VLM and LSL rate estimates of Patton et al. (2017) for the Crescent City and Humboldt Bay tide gauges using a weighted least squares adjustment approach as described by Ghilani (2010) (Table 2, Figure 9). The NHE update work is in progress, but reference to the Patton et al. (2017) work can be made for a general discussion of the tide gauge analysis methods and interpretation of results.

Table 2. Summary of LSL rise and VLM rates for Crescent City and the five Humboldt Bay tide gauges originally developed by Patton et al. (2017), and the weighted least square adjustment values recently developed by NHE (in progress). The weighted least square adjustment provides a mean and standard error (SE) for LSL rise and VLM. Positive VLM rates indicate upward land motion, and negative rates indicate downward motion.

| Tide Gauge Location | Patton et al. (2017) Values | | Weighted Least Squares Adjustment (NHE, in progress) | | | |
|---------------------|--------------------------------|----------------|---|---------------|----------------|---------------|
| | LSL Rise (mm/yr) | VLM (mm/yr) | LSL Rise (mm/yr) | SE (mm/yr) | VLM (mm/yr) | SE (mm/yr) |
| Crescent City | -0.97 | 3.25 | -0.83 | 0.07 | 3.11 | 0.13 |
| North Spit | 4.61 | -2.33 | 4.97 | 0.27 | -2.69 | 0.25 |
| Mad River Slough | 3.39 | -1.11 | 3.32 | 0.53 | -1.04 | 0.27 |
| Samoa | 2.53 | -0.25 | 2.93 | 1.14 | -0.65 | 0.32 |
| Fields Landing | 3.76 | -1.48 | 3.93 | 0.95 | -1.65 | 0.41 |
| Hookton Slough | 5.84 | -3.56 | 5.98 | 0.81 | -3.70 | 0.41 |

The north to south down trending VLM gradient controls the LSL rate variation in Humboldt Bay, with the highest rate of VLM in south Humboldt Bay at the Hookton Slough tide gauge. The tectonic deformation in Humboldt Bay increases the LSL rates well above the long-term GMSL and ReSL rates of 1.7 and 2.28 mm/yr, respectively, with both the North Spit and Hookton Slough LSL rates being more than twice the ReSL rate. These higher LSL rise rates indicate that increases in the GMSL and ReSL will affect Humboldt Bay faster than other parts of U.S. west coast; and within the bay, the south end will be affected sooner than the north end.

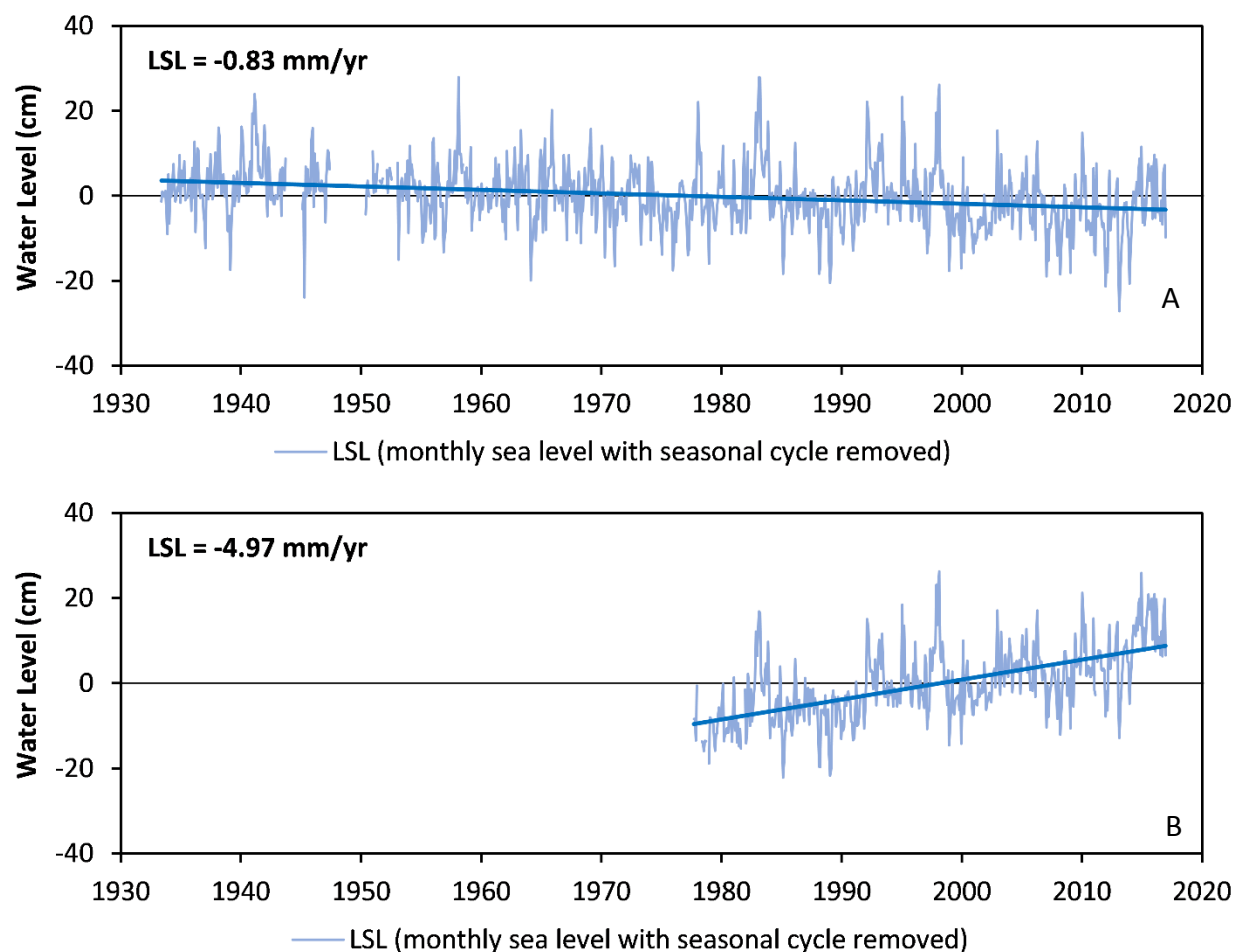


Figure 9. LSL rise trends for (A) Crescent City (1933 to 2016) and (B) North Spit (1977 to 2016) tide gauges using monthly mean sea levels with the average seasonal cycle removed.

Sea-Level Height Variability

Sea-level heights vary due to astronomical tides, storm surge, wind stress effects, changes in barometric pressure, seasonal cycles, and ENSO phases, which results in water levels reaching higher levels over longer time scales (Cayan et al., 2008; Knowles, 2010). Figure 10 shows the hourly water levels for the Crescent City tide gauge for the 1982-83 El Niño years, along with the mean sea level (MSL) and mean higher high water (MHHW) tidal datum, the mean monthly maximum water (MMMW), and the 10- and 100-yr extreme high-water level events.

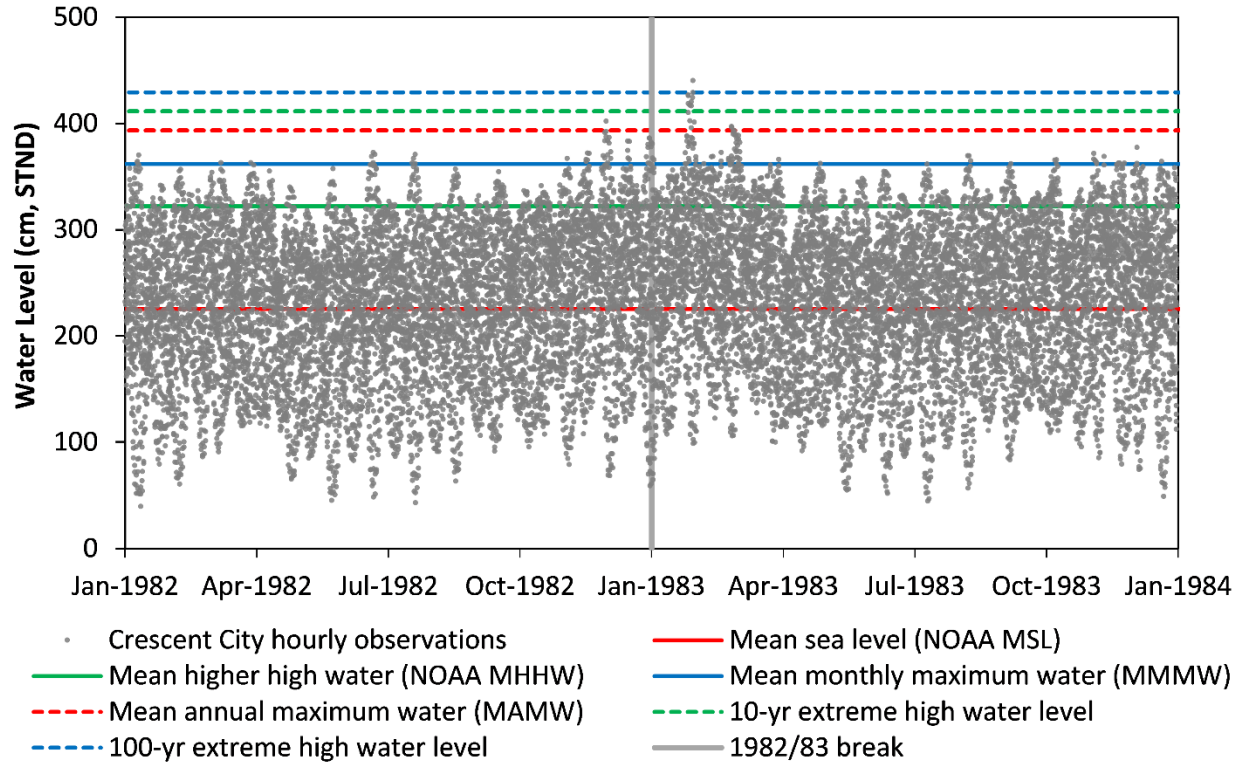


Figure 10. Crescent City tide gauge hourly water levels for 1982-83 El Niño years, with mean sea level (MSL), mean higher high water (MHHW), mean monthly maximum water (MMMW), mean annual maximum water (MAMW), and the 10- and 100-yr extreme high-water level events.

Most coastal damage to the U.S. west coast occurs when storm surge and high waves coincide with high astronomical tides and El Niño events (Cayan et al., 2008; NRC, 2012), which occurred during the winters of 1982-83 and 1997-98. For example, in late January 1983 a large El Niño driven storm coincided with higher than normal astronomical tides, and produced the highest water levels of record at the Crescent City tide gauge on 29 January 1983, exceeding the 100-year extreme exceedance probability event (Figure 10 and Figure 11). The peak hourly water level on 29 January 1983 was 66.2 cm (2.2 ft) higher than the astronomical high tide, and on 26 January 1983, the peak hourly water level was 84.0 cm (2.8 ft) above the astronomical high tide.

It is important to note that sea-level height variability is superimposed onto mean sea level (Cayan et al., 2008). Consequently, as sea-levels rise into the future, the water levels associated with sea-level height variability described above will also increase, and the incidence of extreme high-water levels will become more common (NRC, 2012).

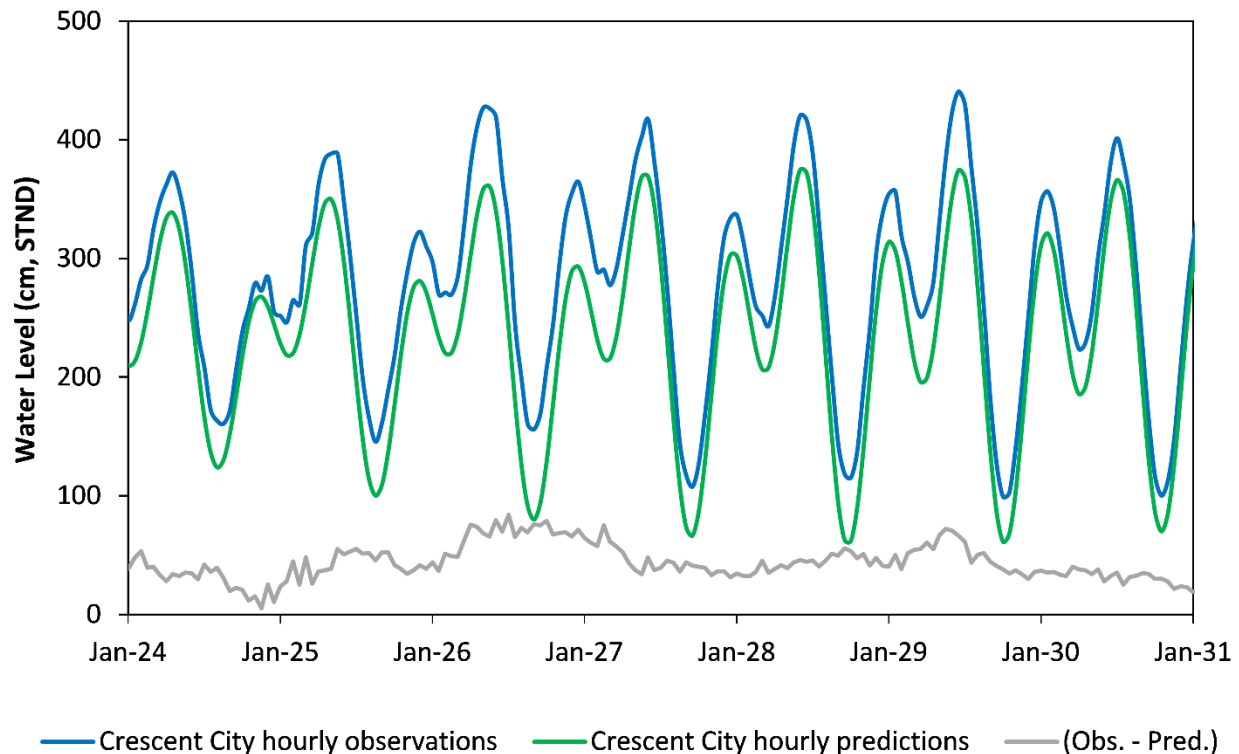


Figure 11. Crescent City tide gauge hourly water levels for January 1983 El Niño year. Blue line is observed water level, green line is astronomical tidal prediction, and grey line is observed minus predicted.

Projections of Sea-Level Rise

Observations provide unequivocal evidence that the climate system is warming and that GMSL has risen over the 20th century (NRC, 2012; IPCC, 2013), but projections of future sea-level rise, including global, regional and local estimates, are necessary to adequately assess and plan for potential impacts to coastal area. Sea-level rise projections generally depend on the understanding of contributions to sea-level change, the response of key geophysical processes, and assumptions regarding future warming of the climate system (NRC, 2012, Church et al., 2013). This section summarizes recent probabilistic projections of GMSL rise, and provides probabilistic estimates of LSL rise for the Humboldt Bay region based on the approach of Kopp et al. (2014).

The NRC (2012) report produced regional projections along the U.S. west coast for three scenarios (low, central and high), with the central or “mid-range” projection having the most weight. The NRC projections covered four regions (Seattle, Newport, San Francisco, and Los Angeles) that varied from the global average due to regional oceanic thermal expansion and dynamics, sea level fingerprint effects, and VLM, and represented the most comprehensive regional projections for the U.S. west coast at the time. Since the NRC (2012) report, significant

effort and advances have been made in developing probabilistic projections of GMSL, ReSL and LSL rise (e.g. Church et al., 2013; Kopp et al., 2014; Grinsted et al., 2015).

The recently released OPC sea-level science update for California (Griggs et al., 2017) used the framework of Kopp et al. (2014) to determine probabilistic sea-level rise projections at three representative locations along the California coast (Crescent City, San Francisco, and La Jolla). Unfortunately, none of these locations adequately represent the high rates of LSL rise occurring in the Humboldt Bay region due to tectonically driven VLM.

The approach of Kopp et al. (2014) provides complete probability distributions for GMSL and LSL rise projections at a global network of tide gauge sites under three emission scenarios, RCP 2.6, RCP 4.5 and RCP 8.5 (discussed below). This approach develops individual probability distributions for the sea-level rise components of glacier/ice cap and ice sheet (Greenland and Antarctic) loss with fingerprint affects, oceanic processes (regional dynamic, thermal and steric effects), land water storage, and VLM from process-based model outputs and expert elicitation for the ice sheets. The GMSL and LSL probability distributions were determined by combining 10,000 Latin hypercube samples (a Monte-Carlo approach) from each individual component distribution. The Kopp et al. (2014) GMSL and LSL projections are available for download as supporting information, and include the Crescent City and North Spit tide gauges.

The IPCC AR5 adopted a set of greenhouse gas emission scenarios known as Representative Concentration Pathways (RCPs), which represent future emissions and concentrations of greenhouse gases, aerosols, and other climate drivers (Church et al., 2013). The RCPs (RCP 8.5, 6.0, 4.5 and 2.6) represent future radiative forcing by 2100 (e.g. RCP 8.5 is 8.5 W/m^2), and are dependent on various mitigation scenarios including implied policy actions, that have different targets in terms of greenhouse gas emissions and radiative forcing (IPCC, 2013). RCP 8.5 is a very high greenhouse gas emission scenario with high radiative forcing, and represents a future where there are no significant efforts to reduce emissions. RCP 2.6 represents an aggressive emission mitigation scenario leading to low radiative forcing, and requires net-negative global emissions in the last quarter of the 21st century. RCP 4.5 and 6.0 represent moderate emission mitigation scenarios. Kopp et al. (2014) only provides projections for RCP 2.6, 4.5 and 8.0, and notes that the sea-level rise projections for RCP 6.0 are similar to those for RCP 4.5.

As discussed in Griggs et al. (2017), recent work on Antarctic Ice Sheet modeling has identified modes of ice-sheet instability that could make extreme sea-level rise more likely than indicated in the Kopp et al. (2014) framework. Consequently, the OPC Science Advisory Team included the extreme sea-level rise scenario (GMSL rise of 2.5 m by 2100) of Sweet et al. (2016) with the Kopp et al. (2014) probabilistic projections. Consistent with Griggs et al. (2017), this extreme scenario (called the H++ scenario) was included in the Humboldt Bay region update, but was renamed the Ext 2.5 scenario to represent the Sweet et al. (2016) extreme GMSL rise of 2.5 m by 2100. The Sweet et al. (2016) scenario projections are also available as supporting information.

The following sections summarize and provide updated sea-level rise projections for the Humboldt Bay region based on the probabilistic projections of Kopp et al. (2014) and the extreme scenario of Sweet et al. (2017), with the local estimates of VLM by Patton et al. (2017) and NHE (in progress) incorporated into the projections.

Global Mean Sea-Level Rise Projections

The GMSL rise projections of Kopp et al. (2014) for the RCP 8.5, RCP 4.5 and RCP 2.6 emission scenarios (Figure 12, Table 3, Table 4) are provided for consistency and comparison with the LSL projections for the Humboldt Bay region. Table 3 show the component contributions to GMSL rise at 2100 for the median (50% probability) and different probability ranges (e.g. 90 and 99% probabilities). The total GMSL median projections and probabilities for 2030, 2050, 2100, 2150 and 2200 are listed in Table 4, along with the Sweet et al. (2016) Ext 2.5 scenario.

It should be noted that the Ext 2.5 scenario, which has unknown probability, is somewhat consistent with the 99.9% probability of the RCP 8.5 projection (Table 4).

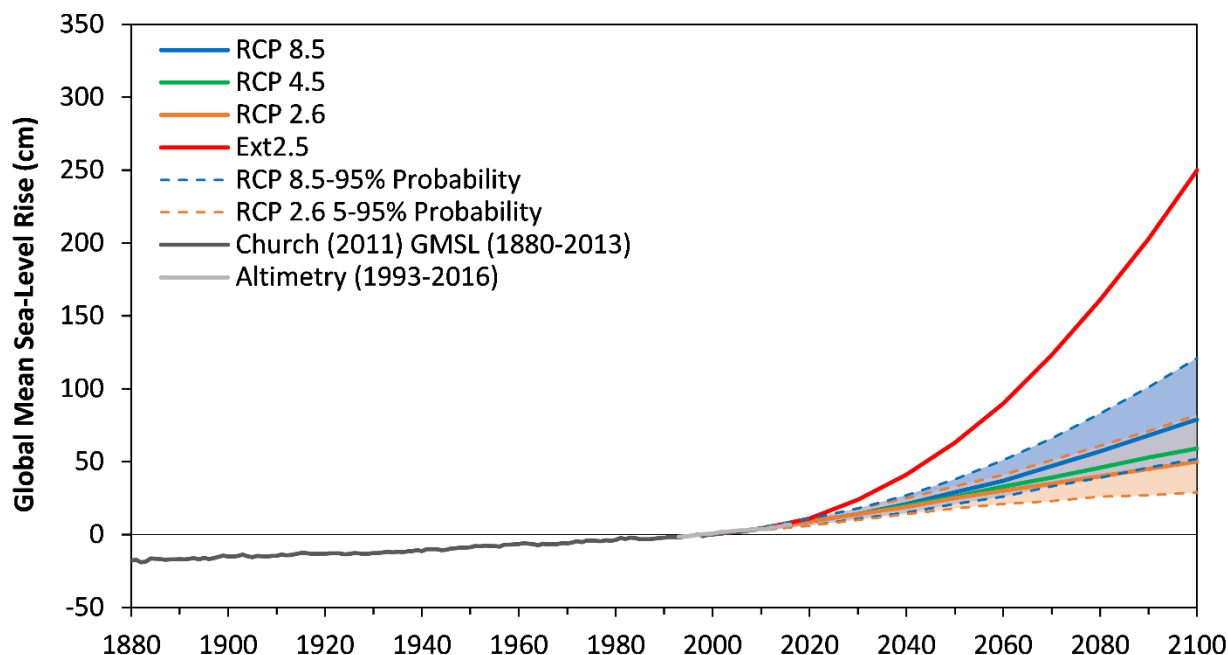


Figure 12. GMSL rise projections at Crescent City for RCP 8.5, RCP 4.5 and RCP 2.6 based on data from Kopp et al. (2014) and the Sweet et al. (2016) extreme scenario of 2.5 m of GMSL rise by 2100 (Ext2.5). The 5 and 95% probabilities are the shaded areas bounded by the dashed lines, and are only shown for RCP 8.5 and RCP 2.6. The reconstructed 1880 to 2013 GMSL curve is from Church et al. (2011). The 1993 to 2016 altimetry data is from Beckley et al. (2010), data downloaded at: <https://sealevel.nasa.gov>. All data relative to year 2000 baseline.

Table 3. GMSL rise component contributions at year 2100 of Kopp et al. (2014). Sea-level values are cm and ft above year 2000 baseline, probabilities are percent.¹

| | RCP 8.5 | | | | | RCP 4.5 | | | | | RCP 2.6 | | | | |
|---------------------------------------|---------|-------------|-------------|-------------|-------|---------|-------------|-------------|-------------|-------|---------|-------------|-------------|-------------|-------|
| | 50 | 17 to 83 | 5 to 95 | 0.5 to 99.5 | 99.9 | 50 | 17 to 83 | 5 to 95 | 0.5 to 99.5 | 99.9 | 50 | 17 to 83 | 5 to 95 | 0.5 to 99.5 | 99.9 |
| Year 2100 – GMSL rise components (cm) | | | | | | | | | | | | | | | |
| GIC | 18 | 14 to 21 | 11 to 24 | 7 to 29 | < 30 | 13 | 10 to 17 | 7 to 19 | 3 to 23 | < 25 | 12 | 9 to 15 | 7 to 17 | 3 to 20 | < 25 |
| GIS | 14 | 8 to 25 | 5 to 39 | 3 to 70 | < 95 | 9 | 4 to 15 | 2 to 23 | 0 to 40 | < 55 | 6 | 4 to 12 | 3 to 17 | 2 to 31 | < 45 |
| AIS | 4 | -8 to 15 | -11 to 33 | -14 to 91 | < 155 | 5 | -5 to 16 | -9 to 33 | -11 to 88 | < 150 | 6 | -4 to 17 | -8 to 35 | -10 to 93 | < 155 |
| TE | 37 | 28 to 46 | 22 to 52 | 12 to 62 | < 65 | 26 | 18 to 34 | 13 to 40 | 4 to 48 | < 55 | 19 | 13 to 26 | 8 to 31 | 1 to 38 | < 40 |
| LWS | 5 | 3 to 7 | 2 to 8 | 0 to 11 | < 10 | 5 | 3 to 7 | 2 to 8 | 0 to 11 | < 10 | 5 | 3 to 7 | 2 to 8 | 0 to 11 | < 10 |
| Total | 79 | 62 to 100 | 52 to 121 | 39 to 176 | < 245 | 59 | 45 to 77 | 36 to 93 | 24 to 147 | < 215 | 50 | 37 to 65 | 29 to 82 | 19 to 141 | < 210 |
| Year 2100 – GMSL rise components (ft) | | | | | | | | | | | | | | | |
| GIC | 0.6 | 0.5 to 0.7 | 0.4 to 0.8 | 0.2 to 1.0 | < 1.0 | 0.4 | 0.3 to 0.6 | 0.2 to 0.6 | 0.1 to 0.8 | < 0.8 | 0.4 | 0.3 to 0.5 | 0.2 to 0.6 | 0.1 to 0.7 | < 0.8 |
| GIS | 0.5 | 0.3 to 0.8 | 0.2 to 1.3 | 0.1 to 2.3 | < 3.1 | 0.3 | 0.1 to 0.5 | 0.1 to 0.8 | 0.0 to 1.3 | < 1.8 | 0.2 | 0.1 to 0.4 | 0.1 to 0.6 | 0.1 to 1.0 | < 1.5 |
| AIS | 0.1 | -0.3 to 0.5 | -0.4 to 1.1 | -0.5 to 3.0 | < 5.1 | 0.2 | -0.2 to 0.5 | -0.3 to 1.1 | -0.4 to 2.9 | < 4.9 | 0.2 | -0.1 to 0.6 | -0.3 to 1.1 | -0.3 to 3.1 | < 5.1 |
| TE | 1.2 | 0.9 to 1.5 | 0.7 to 1.7 | 0.4 to 2.0 | < 2.1 | 0.9 | 0.6 to 1.1 | 0.4 to 1.3 | 0.1 to 1.6 | < 1.8 | 0.6 | 0.4 to 0.9 | 0.3 to 1.0 | 0.0 to 1.2 | < 1.3 |
| LWS | 0.2 | 0.1 to 0.2 | 0.1 to 0.3 | 0.0 to 0.4 | < 0.3 | 0.2 | 0.1 to 0.2 | 0.1 to 0.3 | 0.0 to 0.4 | < 0.3 | 0.2 | 0.1 to 0.2 | 0.1 to 0.3 | 0.0 to 0.4 | < 0.3 |
| Total | 2.6 | 2.0 to 3.3 | 1.7 to 4.0 | 1.3 to 5.8 | < 8.0 | 1.9 | 1.5 to 2.5 | 1.2 to 3.1 | 0.8 to 4.8 | < 7.1 | 1.6 | 1.2 to 2.1 | 1.0 to 2.7 | 0.6 to 4.6 | < 6.9 |

¹GMSL is global mean sea level; GIC is glaciers and ice caps; GIS is Greenland Ice Sheet; AIS is Antarctic Ice Sheet; TE is thermal expansion; LWS is land water storage; and RCP 8.5, RCP 4.5 and RCP 2.6 are greenhouse gas representative concentration pathways of AR5 (IPCC, 2013).

Table 4. GMSL rise projections of Kopp et al. (2014) and the extreme GMSL scenario (2.5 m of GMSL rise by 2100) of Sweet et al. (2016). Sea-level values are cm and ft above year 2000 baseline; probabilities are percent.¹

| | RCP 8.5 | | | | | RCP 4.5 | | | | | RCP 2.6 | | | | | Ext 2.5 |
|-------------------------------|---------|------------|-------------|-------------|--------|---------|------------|------------|-------------|--------|---------|------------|------------|-------------|--------|---------|
| | 50 | 17 to 83 | 5 to 95 | 0.5 to 99.5 | 99.9 | 50 | 17 to 83 | 5 to 95 | 0.5 to 99.5 | 99.9 | 50 | 17 to 83 | 5 to 95 | 0.5 to 99.5 | 99.9 | 50 |
| GMSL projections by year (cm) | | | | | | | | | | | | | | | | |
| 2030 | 14 | 12 to 17 | 11 to 18 | 8 to 21 | < 25 | 14 | 12 to 16 | 10 to 18 | 8 to 20 | < 20 | 14 | 12 to 16 | 10 to 18 | 8 to 20 | < 20 | 24 |
| 2050 | 29 | 24 to 34 | 21 to 38 | 16 to 49 | < 60 | 26 | 21 to 31 | 18 to 35 | 14 to 44 | < 55 | 25 | 21 to 29 | 18 to 33 | 14 to 43 | < 55 | 63 |
| 2100 | 79 | 62 to 100 | 52 to 121 | 39 to 176 | < 245 | 59 | 45 to 77 | 36 to 93 | 24 to 147 | < 215 | 50 | 37 to 65 | 29 to 82 | 19 to 141 | < 210 | 250 |
| 2150 | 130 | 100 to 180 | 80 to 230 | 60 to 370 | < 540 | 90 | 60 to 130 | 40 to 170 | 20 to 310 | < 480 | 70 | 50 to 110 | 30 to 150 | 20 to 290 | < 460 | 550 |
| 2200 | 200 | 130 to 280 | 100 to 370 | 60 to 630 | < 950 | 130 | 70 to 200 | 40 to 270 | 10 to 520 | < 830 | 100 | 50 to 160 | 30 to 240 | 10 to 500 | < 810 | 970 |
| GMSL projections by year (ft) | | | | | | | | | | | | | | | | |
| 2030 | 0.5 | 0.4 to 0.6 | 0.4 to 0.6 | 0.3 to 0.7 | < 0.8 | 0.5 | 0.4 to 0.5 | 0.3 to 0.6 | 0.3 to 0.7 | < 0.7 | 0.5 | 0.4 to 0.5 | 0.3 to 0.6 | 0.3 to 0.7 | < 0.7 | 0.8 |
| 2050 | 1.0 | 0.8 to 1.1 | 0.7 to 1.2 | 0.5 to 1.6 | < 2.0 | 0.9 | 0.7 to 1.0 | 0.6 to 1.1 | 0.5 to 1.4 | < 1.8 | 0.9 | 0.7 to 1.0 | 0.6 to 1.1 | 0.5 to 1.4 | < 1.8 | 2.1 |
| 2100 | 2.6 | 2.0 to 3.3 | 1.7 to 4.0 | 1.3 to 5.8 | < 8.0 | 1.9 | 1.5 to 2.5 | 1.2 to 3.1 | 0.8 to 4.8 | < 7.1 | 1.9 | 1.5 to 2.5 | 1.2 to 3.1 | 0.8 to 4.8 | < 7.1 | 8.2 |
| 2150 | 4.3 | 3.3 to 5.9 | 2.6 to 7.5 | 2.0 to 12.1 | < 17.7 | 3.0 | 2.0 to 4.3 | 1.3 to 5.6 | 0.7 to 10.2 | < 15.7 | 3.0 | 2.0 to 4.3 | 1.3 to 5.6 | 0.7 to 10.2 | < 15.7 | 18.0 |
| 2200 | 6.6 | 4.3 to 9.2 | 3.3 to 12.1 | 2.0 to 20.7 | < 31.2 | 4.3 | 2.3 to 6.6 | 1.3 to 8.9 | 0.3 to 17.1 | < 27.2 | 4.3 | 2.3 to 6.6 | 1.3 to 8.9 | 0.3 to 17.1 | < 27.2 | 31.8 |

¹GMSL is global mean sea level; RCP 8.5, RCP 4.5 and RCP 2.6 are greenhouse gas representative concentration pathways of AR5 (IPCC, 2013); and EXT2.5 is the extreme sea-level rise of 2.5 m of GMSL rise by 2100 of Sweet et al. (2016).

Local Sea-Level Rise Projections for the Humboldt Bay Region

As part of this work, NHE (in progress) updated and/or developed LSL rise probabilistic projections for the RCP 8.5, 4.5 and 2.6 emission scenarios at four sites in the Humboldt Bay region: Crescent City, North Spit, Mad River Slough and Hookton Slough. The three sites in Humboldt Bay (Figure 8) were selected to highlight how the north to south trending VLM gradient affects LSL rise projections.

To provide the LSL rise projections, the Kopp et al. (2014) and Sweet et al. (2016) Ext 2.5 projection data were obtained for the Crescent City and North Spit tide gauges. The VLM contributions to LSL rise for each Kopp et al. (2014) projection were removed (modified Kopp projections), and replaced with the VLM estimates of Patton et al. (2017) as modified by NHE (in progress). Following the same methodology of Kopp et al. (2014), the new VLM probability distributions were determined from 10,000 Latin Hypercube samples assuming a t-distribution with the mean and standard error for the components of the VLM estimates at each site. These VLM probability distributions were combined with the modified Kopp projections to determine LSL rise probabilistic projections for each site. A similar approach was followed for the Ext 2.5 scenario, with the Sweet et al. (2016) projections adjusted with the mean VLM estimate at each site.

For the LSL projections, VLM is configured as a contribution to LSL change. For example, the VLM at North Spit is negative (Table 2) indicating that the ground is moving downward. This downward land motion increases sea-level rise at North Spit, resulting in a positive LSL rise contribution, as reported in the LSL tables. The opposite occurs for Crescent City. Table 5 lists the VLM contributions to LSL change (mean and +/- 2 standard deviations) determined by Kopp et al. (2014) for Crescent City and North Spit, and the NHE (in progress) estimates for these two locations and the Mad River Slough and Hookton Slough sites. The locally generated VLM estimates are higher than those determined by Kopp et al. (2014), which will increase or decrease the updated LSL rates, depending on the site.

Table 5. VLM contributions to LSL change determined by Kopp et al. (2014) and by Patton et al. (2017) and NHE (in progress) used in the updated LSL probability projections for the Humboldt Bay region. VLMs are reported as mean and +/- 2 standard deviations (SD).

| Tide Gauge Location | VLM rate as contribution to LSL change (mm/yr) | | | |
|---------------------|--|----------|--|----------|
| | Kopp et al. (2014) | | Patton et al. (2017) and NHE (in progress) | |
| | Mean | +/- 2 SD | Mean | +/- 2 SD |
| Crescent City | -2.63 | 0.30 | -3.11 | 0.27 |
| Mad River Slough | | | 1.04 | 0.67 |
| North Spit | 1.64 | 0.76 | 2.69 | 0.53 |
| Hookton Slough | | | 3.70 | 1.31 |

The modified LSL projections for Crescent City and North Spit are shown in Figure 13. The 2100 component contributions to LSL rise for Crescent City, North Spit, Mad River Slough and Hookton Slough are provided in Table 6 for the median (50% probability) and different probability ranges (e.g. 90 and 99% probabilities). The total LSL median projection and probabilities at each site for 2030, 2050, 2100, 2150 and 2200 are listed in Table 7, along with the Sweet et al. (2016) extreme scenario (Ext 2.5).

Findings/Discussion

Comparing the 2100 projections for LSL within the Humboldt Bay region to GMSL (Table 3 and Table 6) show differences between GMSL and LSL rise components, and reveal important regional and local factors that affect LSL change compared to GMSL. Within the Humboldt Bay region oceanic dynamic processes appear to have a limited effect on increasing sea levels beyond GMSL projections, except for small increases for the lower RCPs. Contributions from the glaciers/ice caps and Greenland Ice Sheet are projected to be lower than global averages for all RCPs. The Antarctic Ice Sheet is projected to have only slight increases above the global average for the lower RCPs. However, unlike other portions of the U.S. west coast that are projected to have sea-level rise close to the global average (Kopp et al., 2014), the Humboldt Bay region has LSL projections well above the GMSL projections due to tectonically driven VLM.

Crescent City, which is uplifting, has LSL rise projections (50% probability of 0.42 m, 90% probability of 0.11 to 0.88) that are below GMSL projections (50% probability of 0.79 m, 90% probability of 0.52 to 1.21) under RCP 8.5 by 2100. However, North Spit is subsiding, and has LSL projections (50% value of 1.01 m, 90% probability of 0.69 to 1.46) that are above the GMSL projections by 2100 for RCP 8.5. Likewise, Mad River Slough and Hookton Slough also have LSL projections that are above the global average, with Hookton Slough having the highest rates, due to the north to south trending downward VLMs in Humboldt Bay.

It should be noted that up to 2050, differences between LSL projections are minimal between RCP emission scenarios, and the RCP 8.5 projections can just be used (Kopp et al., 2014; Griggs et al., 2017). After 2050, differences in projections begin to emerge due to emission scenarios.

One final note, large interannual monthly and annual mean sea-level variability as occurs in the Humboldt Bay region (Figure 13) can mask LSL rise over the near term (Kopp et al., 2014). The interannual variability also exceeds the uncertainty in projections (~90% probability) until about 2030 to 2040 for annual mean sea levels, and about 2040 to 2050 for monthly mean sea levels. During these timeframes, the interannual variability, either alone or in combination with the LSL rise projections, should be considered in decision making.

The key finding from the updated probabilistic LSL projections is that the tectonically driven VLM in Humboldt Bay creates the highest LSL rise rates in California. These higher LSL rates indicate that GMSL rise will impact Humboldt Bay faster than other parts of the U.S. west coast; and within the bay, the south end will be impacted sooner than the north end.

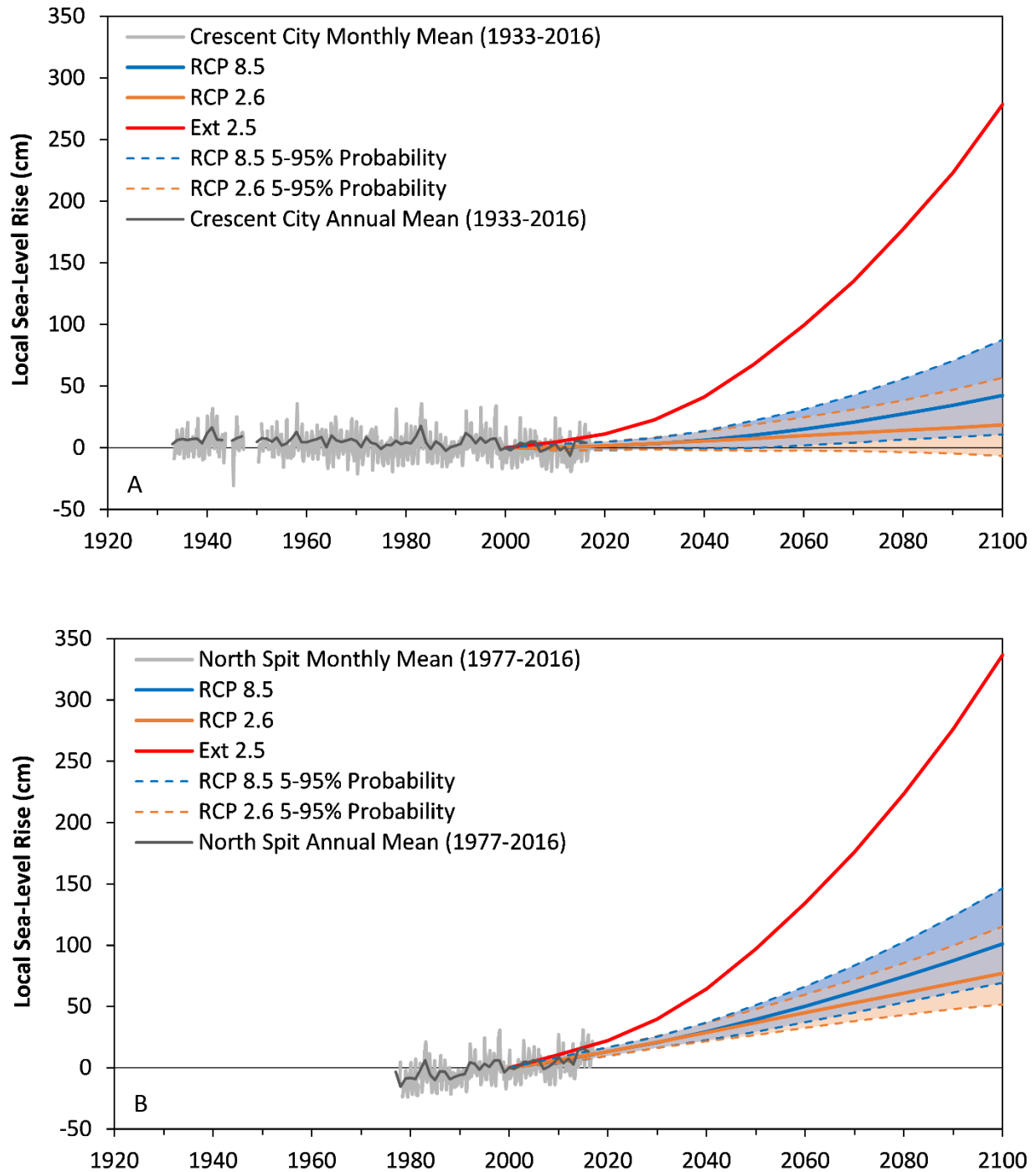


Figure 13. LSL rise projections at Crescent City (A) and North Spit (B) for RCP 8.5 and RCP 2.6 based on data from Kopp et al. (2014), the Sweet et al. (2016) extreme scenario of 2.5 m of GMSL rise by 2100 (Ext 2.5), and VLM contribution to LSL rise by Patton et al. (2017) and NHE (in progress). The 5 and 95 % probabilities are the shaded areas bounded by the dashed lines. The LSL curves are the annual and monthly mean sea levels for the 1933 to 2016 Crescent City data (NOAA 9419750), and the 1977 to 2016 North Spit data (NOAA 9418767), respectively. All data referenced to year 2000 baseline.

Table 6. LSL rise component contributions at year 2100 for Humboldt Bay Region based on data (GIC, GIS, AIS, Ocean and LWS) from Kopp et al. (2014), and VLM contribution to LSL rise by Patton et al. (2017) and NHE (in progress). Sea-level values are cm and ft above year 2000 baseline; probabilities are percent.¹

| | RCP 8.5 | | | | | RCP 4.5 | | | | | RCP 2.6 | | | | |
|--|---------|------------|------------|-------------|-------|---------|------------|------------|-------------|-------|---------|------------|------------|-------------|-------|
| | 50 | 17 to 83 | 5 to 95 | 0.5 to 99.5 | 99.9 | 50 | 17 to 83 | 5 to 95 | 0.5 to 99.5 | 99.9 | 50 | 17 to 83 | 5 to 95 | 0.5 to 99.5 | 99.9 |
| Crescent City, year 2100 – Sea-level rise components (cm) | | | | | | | | | | | | | | | |
| GIC | 13 | 10 to 17 | 8 to 19 | 5 to 22 | < 24 | 10 | 7 to 13 | 5 to 15 | 3 to 18 | < 20 | 9 | 6 to 11 | 5 to 13 | 2 to 16 | < 18 |
| GIS | 12 | 7 to 22 | 4 to 33 | 2 to 59 | < 81 | 8 | 3 to 13 | 2 to 19 | 0 to 34 | < 46 | 5 | 3 to 10 | 2 to 15 | 2 to 26 | < 36 |
| AIS | 4 | -8 to 18 | -13 to 38 | -15 to 110 | < 183 | 6 | -6 to 19 | -10 to 39 | -12 to 106 | < 176 | 7 | -4 to 20 | -8 to 41 | -11 to 112 | < 185 |
| Ocean | 37 | 24 to 49 | 16 to 58 | 2 to 70 | < 77 | 27 | 16 to 39 | 8 to 47 | -4 to 59 | < 64 | 22 | 12 to 32 | 6 to 39 | -5 to 49 | < 54 |
| LWS | 5 | 3 to 7 | 2 to 8 | 0 to 11 | < 12 | 5 | 3 to 7 | 2 to 8 | 0 to 11 | < 12 | 5 | 3 to 7 | 2 to 8 | 0 to 11 | < 12 |
| VLM | -31 | -32 to -30 | -33 to -29 | -35 to -28 | < -27 | -31 | -32 to -30 | -33 to -29 | -35 to -28 | < -27 | -31 | -32 to -30 | -33 to -29 | -35 to -28 | < -27 |
| Total | 42 | 23 to 65 | 11 to 88 | -6 to 155 | < 224 | 26 | 9 to 46 | -2 to 65 | -17 to 131 | < 194 | 18 | 3 to 37 | -7 to 57 | -19 to 125 | < 196 |
| Mad River Slough, year 2100 – Sea-level rise components (cm) | | | | | | | | | | | | | | | |
| GIC | 14 | 11 to 17 | 8 to 19 | 5 to 23 | < 25 | 11 | 8 to 13 | 6 to 15 | 3 to 19 | < 20 | 9 | 7 to 12 | 5 to 14 | 2 to 16 | < 18 |
| GIS | 12 | 7 to 22 | 4 to 34 | 3 to 60 | < 82 | 8 | 3 to 13 | 2 to 20 | 0 to 34 | < 47 | 6 | 3 to 10 | 2 to 15 | 2 to 27 | < 37 |
| AIS | 4 | -8 to 18 | -13 to 39 | -16 to 110 | < 184 | 6 | -6 to 19 | -10 to 39 | -12 to 107 | < 176 | 7 | -4 to 20 | -8 to 41 | -11 to 112 | < 186 |
| Ocean | 37 | 25 to 49 | 16 to 57 | 3 to 69 | < 75 | 27 | 16 to 38 | 9 to 46 | -4 to 58 | < 63 | 22 | 13 to 31 | 6 to 38 | -5 to 48 | < 53 |
| LWS | 5 | 3 to 7 | 2 to 8 | 0 to 11 | < 12 | 5 | 3 to 7 | 2 to 8 | 0 to 11 | < 12 | 5 | 3 to 7 | 2 to 8 | 0 to 11 | < 12 |
| VLM | 10 | 8 to 13 | 5 to 16 | 1 to 20 | < 23 | 10 | 8 to 13 | 5 to 16 | 1 to 20 | < 23 | 10 | 8 to 13 | 5 to 16 | 1 to 20 | < 23 |
| Total | 85 | 65 to 108 | 53 to 130 | 36 to 197 | < 268 | 68 | 51 to 88 | 39 to 108 | 23 to 173 | < 242 | 61 | 45 to 79 | 35 to 99 | 21 to 168 | < 242 |
| North Spit, year 2100 – Sea-level rise components (cm) | | | | | | | | | | | | | | | |
| GIC | 14 | 11 to 17 | 8 to 19 | 5 to 23 | < 25 | 11 | 8 to 13 | 6 to 15 | 3 to 19 | < 20 | 9 | 7 to 12 | 5 to 14 | 2 to 16 | < 18 |
| GIS | 12 | 7 to 22 | 4 to 34 | 3 to 60 | < 82 | 8 | 3 to 13 | 2 to 20 | 0 to 34 | < 47 | 6 | 3 to 10 | 2 to 15 | 2 to 27 | < 37 |
| AIS | 4 | -8 to 18 | -13 to 39 | -16 to 110 | < 184 | 6 | -6 to 19 | -10 to 39 | -12 to 107 | < 176 | 7 | -4 to 20 | -8 to 41 | -11 to 112 | < 186 |
| Ocean | 37 | 25 to 49 | 16 to 57 | 3 to 69 | < 75 | 27 | 16 to 38 | 9 to 46 | -4 to 58 | < 63 | 22 | 13 to 31 | 6 to 38 | -5 to 48 | < 53 |
| LWS | 5 | 3 to 7 | 2 to 8 | 0 to 11 | < 12 | 5 | 3 to 7 | 2 to 8 | 0 to 11 | < 12 | 5 | 3 to 7 | 2 to 8 | 0 to 11 | < 12 |
| VLM | 27 | 24 to 29 | 23 to 31 | 20 to 34 | < 35 | 27 | 24 to 29 | 23 to 31 | 20 to 34 | < 35 | 27 | 24 to 29 | 23 to 31 | 20 to 34 | < 35 |
| Total | 101 | 81 to 124 | 69 to 146 | 53 to 215 | < 287 | 85 | 67 to 104 | 56 to 124 | 41 to 190 | < 252 | 77 | 62 to 95 | 52 to 115 | 39 to 183 | < 253 |
| Hookton Slough, year 2100 – Sea-level rise components (cm) | | | | | | | | | | | | | | | |
| GIC | 14 | 11 to 17 | 8 to 19 | 5 to 23 | < 25 | 11 | 8 to 13 | 6 to 15 | 3 to 19 | < 20 | 9 | 7 to 12 | 5 to 14 | 2 to 16 | < 18 |
| GIS | 12 | 7 to 22 | 4 to 34 | 3 to 60 | < 82 | 8 | 3 to 13 | 2 to 20 | 0 to 34 | < 47 | 6 | 3 to 10 | 2 to 15 | 2 to 27 | < 37 |
| AIS | 4 | -8 to 18 | -13 to 39 | -16 to 110 | < 184 | 6 | -6 to 19 | -10 to 39 | -12 to 107 | < 176 | 7 | -4 to 20 | -8 to 41 | -11 to 112 | < 186 |
| Ocean | 37 | 25 to 49 | 16 to 57 | 3 to 69 | < 75 | 27 | 16 to 38 | 9 to 46 | -4 to 58 | < 63 | 22 | 13 to 31 | 6 to 38 | -5 to 48 | < 53 |
| LWS | 5 | 3 to 7 | 2 to 8 | 0 to 11 | < 12 | 5 | 3 to 7 | 2 to 8 | 0 to 11 | < 12 | 5 | 3 to 7 | 2 to 8 | 0 to 11 | < 12 |
| VLM | 37 | 32 to 42 | 28 to 46 | 16 to 59 | < 73 | 37 | 32 to 42 | 28 to 46 | 16 to 59 | < 73 | 37 | 32 to 42 | 28 to 46 | 16 to 59 | < 73 |
| Total | 111 | 91 to 135 | 79 to 157 | 60 to 224 | < 291 | 94 | 77 to 116 | 65 to 135 | 48 to 199 | < 260 | 87 | 71 to 107 | 61 to 127 | 45 to 193 | < 260 |

Table 6. Continued

| | RCP 8.5 | | | | | RCP 4.5 | | | | | RCP 2.6 | | | | |
|--|---------|--------------|--------------|--------------|--------|---------|--------------|--------------|--------------|--------|---------|--------------|--------------|--------------|--------|
| | 50 | 17 to 83 | 5 to 95 | 0.5 to 99.5 | 99.9 | 50 | 17 to 83 | 5 to 95 | 0.5 to 99.5 | 99.9 | 50 | 17 to 83 | 5 to 95 | 0.5 to 99.5 | 99.9 |
| Crescent City, year 2100 – Sea-level rise components (ft) | | | | | | | | | | | | | | | |
| GIC | 0.4 | 0.3 to 0.6 | 0.3 to 0.6 | 0.2 to 0.7 | < 0.8 | 0.3 | 0.2 to 0.4 | 0.2 to 0.5 | 0.1 to 0.6 | < 0.7 | 0.3 | 0.2 to 0.4 | 0.2 to 0.4 | 0.1 to 0.5 | < 0.6 |
| GIS | 0.4 | 0.2 to 0.7 | 0.1 to 1.1 | 0.1 to 1.9 | < 2.7 | 0.3 | 0.1 to 0.4 | 0.1 to 0.6 | 0.0 to 1.1 | < 1.5 | 0.2 | 0.1 to 0.3 | 0.1 to 0.5 | 0.1 to 0.9 | < 1.2 |
| AIS | 0.1 | -0.3 to 0.6 | -0.4 to 1.2 | -0.5 to 3.6 | < 6.0 | 0.2 | -0.2 to 0.6 | -0.3 to 1.3 | -0.4 to 3.5 | < 5.8 | 0.2 | -0.1 to 0.7 | -0.3 to 1.3 | -0.3 to 3.7 | < 6.1 |
| Ocean | 1.2 | 0.8 to 1.6 | 0.5 to 1.9 | 0.2 to 2.3 | < 2.5 | 0.9 | 0.5 to 1.3 | 0.3 to 1.5 | 0.0 to 1.9 | < 2.1 | 0.7 | 0.4 to 1.0 | 0.2 to 1.3 | -0.1 to 1.6 | < 1.8 |
| LWS | 0.2 | 0.1 to 0.2 | 0.1 to 0.3 | 0.0 to 0.4 | < 0.4 | 0.2 | 0.1 to 0.2 | 0.1 to 0.3 | 0.0 to 0.4 | < 0.4 | 0.2 | 0.1 to 0.2 | 0.1 to 0.3 | 0.0 to 0.4 | < 0.4 |
| VLM | -1.0 | -1.1 to -1.0 | -1.1 to -0.9 | -1.1 to -0.9 | < -0.9 | -1.0 | -1.1 to -1.0 | -1.1 to -0.9 | -1.1 to -0.9 | < -0.9 | -1.0 | -1.1 to -1.0 | -1.1 to -0.9 | -1.1 to -0.9 | < -0.9 |
| Total | 1.4 | 0.7 to 2.1 | 0.4 to 2.9 | -0.1 to 5.1 | < 7.3 | 0.9 | 0.3 to 1.5 | -0.1 to 2.1 | -0.4 to 4.3 | < 6.4 | 0.6 | 0.1 to 1.2 | -0.2 to 1.9 | -0.5 to 4.1 | < 6.4 |
| Mad River Slough, year 2100 – Sea-level rise components (ft) | | | | | | | | | | | | | | | |
| GIC | 0.5 | 0.4 to 0.6 | 0.3 to 0.6 | 0.2 to 0.8 | < 0.8 | 0.4 | 0.3 to 0.4 | 0.2 to 0.5 | 0.1 to 0.6 | < 0.7 | 0.3 | 0.2 to 0.4 | 0.2 to 0.5 | 0.1 to 0.5 | < 0.6 |
| GIS | 0.4 | 0.2 to 0.7 | 0.1 to 1.1 | 0.1 to 2.0 | < 2.7 | 0.3 | 0.1 to 0.4 | 0.1 to 0.7 | 0.0 to 1.1 | < 1.5 | 0.2 | 0.1 to 0.3 | 0.1 to 0.5 | 0.1 to 0.9 | < 1.2 |
| AIS | 0.1 | -0.3 to 0.6 | -0.4 to 1.3 | -0.5 to 3.6 | < 6.0 | 0.2 | -0.2 to 0.6 | -0.3 to 1.3 | -0.4 to 3.5 | < 5.8 | 0.2 | -0.1 to 0.7 | -0.3 to 1.3 | -0.3 to 3.7 | < 6.1 |
| Ocean | 1.2 | 0.8 to 1.6 | 0.5 to 1.9 | 0.2 to 2.3 | < 2.5 | 0.9 | 0.5 to 1.2 | 0.3 to 1.5 | 0.0 to 1.9 | < 2.1 | 0.7 | 0.4 to 1.0 | 0.2 to 1.2 | -0.1 to 1.6 | < 1.7 |
| LWS | 0.2 | 0.1 to 0.2 | 0.1 to 0.3 | 0.0 to 0.4 | < 0.4 | 0.2 | 0.1 to 0.2 | 0.1 to 0.3 | 0.0 to 0.4 | < 0.4 | 0.2 | 0.1 to 0.2 | 0.1 to 0.3 | 0.0 to 0.4 | < 0.4 |
| VLM | 0.3 | 0.2 to 0.4 | 0.2 to 0.5 | 0.1 to 0.7 | < 0.8 | 0.3 | 0.2 to 0.4 | 0.2 to 0.5 | 0.1 to 0.7 | < 0.8 | 0.3 | 0.2 to 0.4 | 0.2 to 0.5 | 0.1 to 0.7 | < 0.8 |
| Total | 2.8 | 2.1 to 3.5 | 1.7 to 4.3 | 1.3 to 6.5 | < 8.8 | 2.2 | 1.7 to 2.9 | 1.3 to 3.5 | 0.9 to 5.7 | < 7.9 | 2.0 | 1.5 to 2.6 | 1.1 to 3.2 | 0.8 to 5.5 | < 7.9 |
| North Spit, year 2100 – Sea-level rise components (ft) | | | | | | | | | | | | | | | |
| GIC | 0.5 | 0.4 to 0.6 | 0.3 to 0.6 | 0.2 to 0.8 | < 0.8 | 0.4 | 0.3 to 0.4 | 0.2 to 0.5 | 0.1 to 0.6 | < 0.7 | 0.3 | 0.2 to 0.4 | 0.2 to 0.5 | 0.1 to 0.5 | < 0.6 |
| GIS | 0.4 | 0.2 to 0.7 | 0.1 to 1.1 | 0.1 to 2.0 | < 2.7 | 0.3 | 0.1 to 0.4 | 0.1 to 0.7 | 0.0 to 1.1 | < 1.5 | 0.2 | 0.1 to 0.3 | 0.1 to 0.5 | 0.1 to 0.9 | < 1.2 |
| AIS | 0.1 | -0.3 to 0.6 | -0.4 to 1.3 | -0.5 to 3.6 | < 6.0 | 0.2 | -0.2 to 0.6 | -0.3 to 1.3 | -0.4 to 3.5 | < 5.8 | 0.2 | -0.1 to 0.7 | -0.3 to 1.3 | -0.3 to 3.7 | < 6.1 |
| Ocean | 1.2 | 0.8 to 1.6 | 0.5 to 1.9 | 0.2 to 2.3 | < 2.5 | 0.9 | 0.5 to 1.2 | 0.3 to 1.5 | 0.0 to 1.9 | < 2.1 | 0.7 | 0.4 to 1.0 | 0.2 to 1.2 | -0.1 to 1.6 | < 1.7 |
| LWS | 0.2 | 0.1 to 0.2 | 0.1 to 0.3 | 0.0 to 0.4 | < 0.4 | 0.2 | 0.1 to 0.2 | 0.1 to 0.3 | 0.0 to 0.4 | < 0.4 | 0.2 | 0.1 to 0.2 | 0.1 to 0.3 | 0.0 to 0.4 | < 0.4 |
| VLM | 0.9 | 0.8 to 1.0 | 0.7 to 1.0 | 0.7 to 1.1 | < 1.2 | 0.9 | 0.8 to 1.0 | 0.7 to 1.0 | 0.7 to 1.1 | < 1.2 | 0.9 | 0.8 to 1.0 | 0.7 to 1.0 | 0.7 to 1.1 | < 1.2 |
| Total | 3.3 | 2.7 to 4.1 | 2.3 to 4.8 | 1.9 to 7.0 | < 9.4 | 2.8 | 2.2 to 3.4 | 1.8 to 4.1 | 1.5 to 6.2 | < 8.3 | 2.5 | 2.0 to 3.1 | 1.7 to 3.8 | 1.4 to 6.0 | < 8.3 |
| Hookton Slough, year 2100 – Sea-level rise components (ft) | | | | | | | | | | | | | | | |
| GIC | 0.5 | 0.4 to 0.6 | 0.3 to 0.6 | 0.2 to 0.8 | < 0.8 | 0.4 | 0.3 to 0.4 | 0.2 to 0.5 | 0.1 to 0.6 | < 0.7 | 0.3 | 0.2 to 0.4 | 0.2 to 0.5 | 0.1 to 0.5 | < 0.6 |
| GIS | 0.4 | 0.2 to 0.7 | 0.1 to 1.1 | 0.1 to 2.0 | < 2.7 | 0.3 | 0.1 to 0.4 | 0.1 to 0.7 | 0.0 to 1.1 | < 1.5 | 0.2 | 0.1 to 0.3 | 0.1 to 0.5 | 0.1 to 0.9 | < 1.2 |
| AIS | 0.1 | -0.3 to 0.6 | -0.4 to 1.3 | -0.5 to 3.6 | < 6.0 | 0.2 | -0.2 to 0.6 | -0.3 to 1.3 | -0.4 to 3.5 | < 5.8 | 0.2 | -0.1 to 0.7 | -0.3 to 1.3 | -0.3 to 3.7 | < 6.1 |
| Ocean | 1.2 | 0.8 to 1.6 | 0.5 to 1.9 | 0.2 to 2.3 | < 2.5 | 0.9 | 0.5 to 1.2 | 0.3 to 1.5 | 0.0 to 1.9 | < 2.1 | 0.7 | 0.4 to 1.0 | 0.2 to 1.2 | -0.1 to 1.6 | < 1.7 |
| LWS | 0.2 | 0.1 to 0.2 | 0.1 to 0.3 | 0.0 to 0.4 | < 0.4 | 0.2 | 0.1 to 0.2 | 0.1 to 0.3 | 0.0 to 0.4 | < 0.4 | 0.2 | 0.1 to 0.2 | 0.1 to 0.3 | 0.0 to 0.4 | < 0.4 |
| VLM | 1.2 | 1.1 to 1.4 | 0.9 to 1.5 | 0.6 to 2.0 | < 2.4 | 1.2 | 1.1 to 1.4 | 0.9 to 1.5 | 0.6 to 2.0 | < 2.4 | 1.2 | 1.1 to 1.4 | 0.9 to 1.5 | 0.6 to 2.0 | < 2.4 |
| Total | 3.6 | 3.0 to 4.4 | 2.6 to 5.2 | 2.2 to 7.4 | < 9.6 | 3.1 | 2.5 to 3.8 | 2.1 to 4.4 | 1.8 to 6.5 | < 8.5 | 2.8 | 2.3 to 3.5 | 2.0 to 4.2 | 1.6 to 6.3 | < 8.5 |

¹LSL is local sea level; VLM is vertical land motion contribution to LSL; GIC is glaciers and ice caps; GIS is Greenland Ice Sheet; AIS is Antarctic Ice Sheet; Ocean is ocean thermal, steric and dynamic contribution; LWS is land water storage; RCP 8.5, RCP 4.5 and RCP 2.6 are greenhouse gas representative concentration pathways of AR5 (IPCC, 2013).

Table 7. LSL rise projections for Humboldt Bay Region based on data from Kopp et al. (2014), the extreme GMSL scenario (2.5 m of GMSL rise by 2100) of Sweet et al. (2016), and VLM contribution to LSL rise by Patton et al. (2017) and NHE (in progress). Sea-level values are cm and ft above year 2000 baseline; probabilities are percent.¹

| | RCP 8.5 | | | | | RCP 4.5 | | | | | RCP 2.6 | | | | | Ext 2.5 |
|--|---------|------------|------------|-------------|--------|---------|------------|------------|-------------|-------|---------|------------|------------|-------------|-------|---------|
| | 50 | 17 to 83 | 5 to 95 | 0.5 to 99.5 | 99.9 | 50 | 17 to 83 | 5 to 95 | 0.5 to 99.5 | 99.9 | 50 | 17 to 83 | 5 to 95 | 0.5 to 99.5 | 99.9 | 50 |
| Crescent City LSL rise projections by year (cm) | | | | | | | | | | | | | | | | |
| 2030 | 3 | 1 to 6 | -1 to 8 | -4 to 11 | < 14 | 3 | 0 to 6 | -3 to 9 | -6 to 13 | < 15 | 3 | 1 to 6 | -1 to 8 | -4 to 12 | < 14 | 23 |
| 2050 | 10 | 4 to 17 | 0 to 22 | -6 to 33 | < 50 | 9 | 3 to 15 | -2 to 20 | -8 to 30 | < 46 | 8 | 2 to 14 | -2 to 19 | -8 to 30 | < 47 | 68 |
| 2100 | 42 | 23 to 65 | 11 to 88 | -6 to 155 | < 224 | 26 | 9 to 46 | -2 to 65 | -17 to 131 | < 194 | 18 | 3 to 37 | -7 to 57 | -19 to 125 | < 196 | 279 |
| 2150 | 75 | 40 to 122 | 20 to 176 | -2 to 333 | < 507 | 43 | 10 to 84 | -10 to 130 | -35 to 288 | < 452 | 25 | -4 to 62 | -17 to 111 | -31 to 281 | < 458 | 620 |
| 2200 | 118 | 54 to 205 | 19 to 305 | -19 to 597 | < 904 | 62 | 4 to 135 | -28 to 220 | -66 to 511 | < 804 | 34 | -18 to 102 | -41 to 193 | -63 to 505 | < 810 | 1062 |
| Mad River Slough LSL rise projections by year (cm) | | | | | | | | | | | | | | | | |
| 2030 | 16 | 13 to 19 | 11 to 21 | 9 to 24 | < 26 | 16 | 12 to 19 | 10 to 22 | 6 to 25 | < 28 | 16 | 13 to 19 | 11 to 21 | 8 to 25 | < 27 | 35 |
| 2050 | 31 | 25 to 38 | 21 to 43 | 15 to 54 | < 71 | 30 | 23 to 36 | 19 to 41 | 13 to 51 | < 67 | 29 | 23 to 35 | 18 to 40 | 12 to 51 | < 67 | 89 |
| 2100 | 85 | 65 to 108 | 53 to 130 | 36 to 197 | < 268 | 68 | 51 to 88 | 39 to 108 | 23 to 173 | < 242 | 61 | 45 to 79 | 35 to 99 | 21 to 168 | < 242 | 320 |
| 2150 | 139 | 103 to 187 | 83 to 241 | 60 to 399 | < 565 | 106 | 73 to 148 | 53 to 194 | 28 to 349 | < 511 | 88 | 59 to 126 | 45 to 175 | 30 to 343 | < 518 | 685 |
| 2200 | 203 | 138 to 290 | 102 to 392 | 64 to 684 | < 993 | 146 | 87 to 219 | 54 to 304 | 17 to 598 | < 891 | 118 | 66 to 187 | 41 to 279 | 20 to 586 | < 887 | 1149 |
| North Spit LSL rise projections by year (cm) | | | | | | | | | | | | | | | | |
| 2030 | 21 | 18 to 23 | 16 to 25 | 14 to 29 | < 31 | 21 | 17 to 24 | 15 to 26 | 11 to 30 | < 32 | 21 | 18 to 24 | 16 to 26 | 13 to 29 | < 31 | 40 |
| 2050 | 40 | 33 to 46 | 29 to 51 | 24 to 62 | < 80 | 38 | 32 to 44 | 28 to 49 | 22 to 60 | < 74 | 37 | 31 to 43 | 27 to 48 | 21 to 59 | < 74 | 97 |
| 2100 | 101 | 81 to 124 | 69 to 146 | 53 to 215 | < 287 | 85 | 67 to 104 | 56 to 124 | 41 to 190 | < 252 | 77 | 62 to 95 | 52 to 115 | 39 to 183 | < 253 | 337 |
| 2150 | 163 | 127 to 211 | 107 to 265 | 85 to 427 | < 597 | 131 | 97 to 173 | 77 to 219 | 53 to 379 | < 547 | 112 | 84 to 150 | 70 to 200 | 54 to 365 | < 547 | 710 |
| 2200 | 236 | 171 to 323 | 136 to 424 | 96 to 717 | < 1024 | 178 | 120 to 252 | 88 to 337 | 48 to 625 | < 922 | 150 | 99 to 219 | 76 to 310 | 52 to 617 | < 927 | 1182 |
| Hookton Slough LSL rise projections by year (cm) | | | | | | | | | | | | | | | | |
| 2030 | 24 | 21 to 27 | 19 to 29 | 15 to 33 | < 36 | 24 | 20 to 27 | 17 to 30 | 13 to 34 | < 37 | 24 | 21 to 27 | 18 to 30 | 14 to 34 | < 37 | 43 |
| 2050 | 45 | 38 to 52 | 33 to 57 | 26 to 70 | < 88 | 43 | 36 to 50 | 32 to 55 | 25 to 67 | < 83 | 42 | 35 to 49 | 31 to 54 | 23 to 67 | < 83 | 102 |
| 2100 | 111 | 91 to 135 | 79 to 157 | 60 to 224 | < 291 | 94 | 77 to 116 | 65 to 135 | 48 to 199 | < 260 | 87 | 71 to 107 | 61 to 127 | 45 to 193 | < 260 | 347 |
| 2150 | 179 | 142 to 227 | 121 to 282 | 96 to 436 | < 605 | 147 | 112 to 189 | 92 to 235 | 64 to 395 | < 555 | 128 | 99 to 166 | 83 to 215 | 65 to 386 | < 560 | 725 |
| 2200 | 256 | 191 to 345 | 154 to 445 | 114 to 741 | < 1049 | 199 | 140 to 273 | 106 to 358 | 66 to 648 | < 947 | 171 | 119 to 241 | 95 to 332 | 66 to 634 | < 950 | 1202 |

Table 7. Continued

| | RCP 8.5 | | | | | RCP 4.5 | | | | | RCP 2.6 | | | | | Ext 2.5 |
|--|---------|-------------|-------------|--------------|--------|---------|------------|-------------|--------------|--------|---------|-------------|-------------|--------------|--------|---------|
| | 50 | 17 to 83 | 5 to 95 | 0.5 to 99.5 | 99.9 | 50 | 17 to 83 | 5 to 95 | 0.5 to 99.5 | 99.9 | 50 | 17 to 83 | 5 to 95 | 0.5 to 99.5 | 99.9 | 50 |
| Crescent City LSL rise projections by year (ft) | | | | | | | | | | | | | | | | |
| 2030 | 0.1 | 0.0 to 0.2 | 0.0 to 0.3 | -0.1 to 0.4 | < 0.4 | 0.1 | 0.0 to 0.2 | -0.1 to 0.3 | -0.2 to 0.4 | < 0.5 | 0.1 | 0.0 to 0.2 | 0.0 to 0.3 | -0.1 to 0.4 | < 0.5 | 0.7 |
| 2050 | 0.3 | 0.1 to 0.5 | 0.0 to 0.7 | -0.2 to 1.1 | < 1.7 | 0.3 | 0.1 to 0.5 | -0.1 to 0.7 | -0.2 to 1.0 | < 1.5 | 0.2 | 0.1 to 0.5 | -0.1 to 0.6 | -0.2 to 1.0 | < 1.5 | 2.2 |
| 2100 | 1.4 | 0.7 to 2.1 | 0.4 to 2.9 | -0.1 to 5.1 | < 7.3 | 0.9 | 0.3 to 1.5 | -0.1 to 2.1 | -0.4 to 4.3 | < 6.4 | 0.6 | 0.1 to 1.2 | -0.2 to 1.9 | -0.5 to 4.1 | < 6.4 | 9.1 |
| 2150 | 2.5 | 1.3 to 4.0 | 0.7 to 5.8 | 0.1 to 10.9 | < 16.6 | 1.4 | 0.3 to 2.8 | -0.3 to 4.3 | -0.9 to 9.4 | < 14.8 | 0.8 | -0.1 to 2.0 | -0.5 to 3.6 | -0.9 to 9.2 | < 15.0 | 20.4 |
| 2200 | 3.9 | 1.8 to 6.7 | 0.6 to 10.0 | -0.3 to 19.6 | < 29.7 | 2.0 | 0.1 to 4.4 | -0.9 to 7.2 | -1.9 to 16.8 | < 26.4 | 1.1 | -0.6 to 3.4 | -1.3 to 6.3 | -1.9 to 16.6 | < 26.6 | 34.8 |
| Mad River Slough LSL rise projections by year (ft) | | | | | | | | | | | | | | | | |
| 2030 | 0.5 | 0.4 to 0.6 | 0.4 to 0.7 | 0.3 to 0.8 | < 0.9 | 0.5 | 0.4 to 0.6 | 0.3 to 0.7 | 0.2 to 0.8 | < 0.9 | 0.5 | 0.4 to 0.6 | 0.4 to 0.7 | 0.3 to 0.8 | < 0.9 | 1.1 |
| 2050 | 1.0 | 0.8 to 1.2 | 0.7 to 1.4 | 0.6 to 1.8 | < 2.3 | 1.0 | 0.8 to 1.2 | 0.6 to 1.3 | 0.5 to 1.7 | < 2.2 | 0.9 | 0.7 to 1.1 | 0.6 to 1.3 | 0.5 to 1.7 | < 2.2 | 2.9 |
| 2100 | 2.8 | 2.1 to 3.5 | 1.7 to 4.3 | 1.3 to 6.5 | < 8.8 | 2.2 | 1.7 to 2.9 | 1.3 to 3.5 | 0.9 to 5.7 | < 7.9 | 2.0 | 1.5 to 2.6 | 1.1 to 3.2 | 0.8 to 5.5 | < 7.9 | 10.5 |
| 2150 | 4.5 | 3.4 to 6.1 | 2.7 to 7.9 | 2.1 to 13.1 | < 18.5 | 3.5 | 2.4 to 4.9 | 1.7 to 6.4 | 1.1 to 11.5 | < 16.8 | 2.9 | 1.9 to 4.1 | 1.5 to 5.7 | 1.1 to 11.2 | < 17.0 | 22.5 |
| 2200 | 6.6 | 4.5 to 9.5 | 3.3 to 12.9 | 2.4 to 22.4 | < 32.6 | 4.8 | 2.9 to 7.2 | 1.8 to 10.0 | 0.8 to 19.6 | < 29.2 | 3.9 | 2.2 to 6.1 | 1.4 to 9.2 | 0.8 to 19.2 | < 29.1 | 37.7 |
| North Spit LSL rise projections by year (ft) | | | | | | | | | | | | | | | | |
| 2030 | 0.7 | 0.6 to 0.8 | 0.5 to 0.8 | 0.5 to 0.9 | < 1.0 | 0.7 | 0.6 to 0.8 | 0.5 to 0.9 | 0.4 to 1.0 | < 1.1 | 0.7 | 0.6 to 0.8 | 0.5 to 0.8 | 0.5 to 1.0 | < 1.0 | 1.3 |
| 2050 | 1.3 | 1.1 to 1.5 | 1.0 to 1.7 | 0.8 to 2.0 | < 2.6 | 1.2 | 1.0 to 1.4 | 0.9 to 1.6 | 0.8 to 2.0 | < 2.4 | 1.2 | 1.0 to 1.4 | 0.9 to 1.6 | 0.7 to 1.9 | < 2.4 | 3.2 |
| 2100 | 3.3 | 2.7 to 4.1 | 2.3 to 4.8 | 1.9 to 7.0 | < 9.4 | 2.8 | 2.2 to 3.4 | 1.8 to 4.1 | 1.5 to 6.2 | < 8.3 | 2.5 | 2.0 to 3.1 | 1.7 to 3.8 | 1.4 to 6.0 | < 8.3 | 11.0 |
| 2150 | 5.4 | 4.2 to 6.9 | 3.5 to 8.7 | 3.0 to 14.0 | < 19.6 | 4.3 | 3.2 to 5.7 | 2.5 to 7.2 | 1.9 to 12.4 | < 17.9 | 3.7 | 2.8 to 4.9 | 2.3 to 6.5 | 1.9 to 12.0 | < 17.9 | 23.3 |
| 2200 | 7.7 | 5.6 to 10.6 | 4.5 to 13.9 | 3.5 to 23.5 | < 33.6 | 5.8 | 3.9 to 8.3 | 2.9 to 11.1 | 1.9 to 20.5 | < 30.3 | 4.9 | 3.2 to 7.2 | 2.5 to 10.2 | 1.9 to 20.2 | < 30.4 | 38.8 |
| Hookton Slough LSL rise projections by year (ft) | | | | | | | | | | | | | | | | |
| 2030 | 0.8 | 0.7 to 0.9 | 0.6 to 1.0 | 0.5 to 1.1 | < 1.2 | 0.8 | 0.7 to 0.9 | 0.6 to 1.0 | 0.5 to 1.1 | < 1.2 | 0.8 | 0.7 to 0.9 | 0.6 to 1.0 | 0.5 to 1.1 | < 1.2 | 1.4 |
| 2050 | 1.5 | 1.2 to 1.7 | 1.1 to 1.9 | 0.9 to 2.3 | < 2.9 | 1.4 | 1.2 to 1.6 | 1.0 to 1.8 | 0.9 to 2.2 | < 2.7 | 1.4 | 1.2 to 1.6 | 1.0 to 1.8 | 0.8 to 2.2 | < 2.7 | 3.3 |
| 2100 | 3.6 | 3.0 to 4.4 | 2.6 to 5.2 | 2.2 to 7.4 | < 9.6 | 3.1 | 2.5 to 3.8 | 2.1 to 4.4 | 1.8 to 6.5 | < 8.5 | 2.8 | 2.3 to 3.5 | 2.0 to 4.2 | 1.6 to 6.3 | < 8.5 | 11.4 |
| 2150 | 5.9 | 4.7 to 7.4 | 4.0 to 9.3 | 3.4 to 14.3 | < 19.8 | 4.8 | 3.7 to 6.2 | 3.0 to 7.7 | 2.4 to 13.0 | < 18.2 | 4.2 | 3.2 to 5.5 | 2.7 to 7.1 | 2.3 to 12.7 | < 18.4 | 23.8 |
| 2200 | 8.4 | 6.3 to 11.3 | 5.1 to 14.6 | 4.1 to 24.3 | < 34.4 | 6.5 | 4.6 to 9.0 | 3.5 to 11.8 | 2.5 to 21.2 | < 31.1 | 5.6 | 3.9 to 7.9 | 3.1 to 10.9 | 2.4 to 20.8 | < 31.2 | 39.4 |

¹LSL is local sea level; RCP 8.5, RCP 4.5 and RCP 2.6 are greenhouse gas representative concentration pathways of AR5 (IPCC, 2013); and Ext 2.5 is the extreme 2.5 m of GMSL rise by 2100 of Sweet et al. (2016).

Glossary

| | |
|--------|---|
| AIS | Antarctic Ice Sheet |
| AR5 | IPCC Fifth Assessment Report |
| CG | Cascadia Geosciences |
| CSZ | Cascadia subduction zone |
| ENSO | El Niño Southern Oscillation |
| GIA | glacial isostatic adjustment |
| GIC | glaciers and ice caps |
| GIS | Greenland Ice Sheet |
| GMSL | global mean sea level |
| GPS | global positioning system |
| IPCC | Intergovernmental Panel on Climate Change |
| LSL | local sea-level |
| LWS | land water storage |
| MAMW | mean annual maximum water |
| MEI | multivariate ENSO index |
| MHHW | mean higher high water |
| MMMW | mean monthly maximum water |
| MSL | mean sea level |
| NAVD88 | North American Vertical Datum of 1988 |
| NHE | Northern Hydrology and Engineering |
| NOAA | National Ocean and Atmospheric Administration |
| OPC | Ocean Protection Council |
| PDO | Pacific Decadal Oscillation |
| PNW | U.S. Pacific Northwest |
| RCP | representative concentration pathway |
| ReSL | regional sea-level |
| TE | thermal expansion |
| VLM | vertical land motion |

References

- Beckley, B.D., N.P. Zelensky, S.A. Holmes, F.G. Lemoine, R.D. Ray, G.T. Mitchum, S.D. Desai, and S.T. Brown. 2010. Assessment of the Jason-2 Extension to the TOPEX/Poseidon, Jason-1 Sea-Surface Height Time Series for Global Mean Sea Level Monitoring. *Marine Geodesy*, Vol 33, Suppl 1.
- Bromirski, P. D., A. J. Miller, R. E. Flick, and G. Auad. 2011. Dynamical suppression of sea level rise along the Pacific coast of North America: Indications for imminent acceleration. *J. Geophys. Res.*, 116, C07005.
- Burgette, R. J., R. J. Weldon II, and D. A. Schmidt. 2009. Interseismic uplift rates for western Oregon and along-strike variation in locking on the Cascadia subduction zone. *J. Geophys. Res.*, 114, B01408.
- Cayan D. R., P. D. Bromirski, K. Hayhoe, M. Tyree, M. D. Dettinger, and R. E. Flick. 2008. Climate change projections of sea level extremes along the California coast. *Climatic Change*, 87, 57–73.
- Church, J. A. and N.J. White. 2006. A 20th century acceleration in global sea level rise, *Geophysical Research Letters*, 33, L01602.
- Church, J. A., and N. J. White. 2011. Sea-level rise from the late 19th to the early 21st century. *Surv. Geophys.*, 32, 585–602.
- Church, J.A., P.U. Clark, A. Cazenave, J.M. Gregory, S. Jevrejeva, A. Levermann, M.A. Merrifield, G.A. Milne, R.S. Nerem, P.D. Nunn, A.J. Payne, W.T. Pfeffer, D. Stammer and A.S. Unnikrishnan. 2013. Sea Level Change. In: *Climate Change 2013: The Physical Science Basis. Contribution of Working Group I to the Fifth Assessment Report of the Intergovernmental Panel on Climate Change* [Stocker, T.F., D. Qin, G.-K. Plattner, M. Tignor, S.K. Allen, J. Boschung, A. Nauels, Y. Xia, V. Bex and P.M. Midgley (eds.)]. Cambridge University Press, Cambridge, United Kingdom and New York, NY, USA.
- Ghilani, C. D. 2010. *Adjustment Computations Spatial Data Analysis, Fifth Edition*. John Wiley & Sons, Inc. New Jersey.
- Griggs, G, J. Árvai, D. Cayan, R. DeConto, J. Fox, H.A. Fricker, R.E. Kopp, C. Tebaldi, and E.A. Whiteman. 2017. Rising Seas in California: An Update on Sea-Level Rise Science. California Ocean Science Trust.
- Grinsted, A., S. Jevrejeva, R.E.M Riccardo, and D. Dahl-Jensen. 2015. Sea level rise projections for northern Europe under RCP8.5. *Clim. Res.*, 64:15-23.
- Hall, J.A., S. Gill, J. Obeysekera, W. Sweet, K. Knuuti, and J. Marburger. 2016. Regional Sea Level Scenarios for Coastal Risk Management: Managing the Uncertainty of Future Sea Level

- Change and Extreme Water Levels for Department of Defense Coastal Sites Worldwide. U.S. Department of Defense, Strategic Environmental Research and Development Program. 224 pp.
- Hamlington, B.D., S.H. Cheon, P.R. Thompson, M.A. Merrifield, R.S. Nerem, R.R. Leben, and K.Y. Kim. 2016. An ongoing shift in Pacific Ocean sea level. *Journal of Geophysical Research: Oceans*, 121(7), 5084-5097.
- Hay, C.C., E. Morrow, R.E. Kopp, and J.X. Mitrovica. 2015. Probabilistic reanalysis of twentieth-century sea-level rise. *Nature*, 517(7535), 481-484.
- IPCC. 2013. Summary for Policymakers. In: Climate Change 2013: The Physical Science Basis. Contribution of Working Group I to the Fifth Assessment Report of the Intergovernmental Panel on Climate Change [Stocker, T.F., D. Qin, G.-K. Plattner, M. Tignor, S.K. Allen, J. Boschung, A. Nauels, Y. Xia, V. Bex and P.M. Midgley (eds.)]. Cambridge University Press, Cambridge, United Kingdom and New York, NY, USA.
- Knowles, N. 2010. Potential inundation due to rising sea levels in the San Francisco bay region. *San Francisco Estuary and Watershed Science*, 8(1).
- Komar, P. D., J.C. Allan, and P. Ruggiero. 2011. Sea level variations along the U.S. Pacific Northwest Coast: tectonic and climate controls. *Journal of Coastal Research: Volume 27, Issue 5*: pp. 808 – 823.
- Kominz, M. 2001. Sea Level Variations Over Geologic Time. In Encyclopedia of Ocean Sciences. Elsevier, 2605-2613.
- Kopp, R.E., R.M. Horton, C.M. Little, J.X. Mitrovica, M. Oppenheimer, D.J. Rasmussen, B.H. Strauss, and C. Tebaldi. 2014. Probabilistic 21st and 22nd Century Sea-Level Projections at a Global Network of Tide-Gauge Sites. *Earth's Future*, 2:1–24.
- Kopp, R.E., B.P. Horton, A.C. Kemp, and C. Tebaldi. 2015. Past and Future Sea-Level Rise along the Coast of North Carolina, USA. *Climatic Change*, 132:693–707.
- Laird, A. 2013. Humboldt Bay Shoreline Inventory, Mapping and Sea Level Rise Vulnerability Assessment. Prepared for State Coastal Conservancy. Trinity Associates, Arcata, CA.
- Mantua, N. J., S. R. Hare, Y. Zhang, J. M. Wallace, and R.C. Francis. 1997. A Pacific interdecadal climate oscillation with impacts on salmon production. *Bulletin of the American Meteorological Society*, 78, 1069-1079.
- Mitchell, C. E., P. Vincent, R. J. Weldon, and M. A. Richards. 1994. Present-day vertical deformation of the Cascadia margin, Pacific northwest, United States: *J. Geophys. Res.* 99(B6), 12,257-12,277.
- National Research Council (NRC). 2012. Sea-Level Rise for the Coasts of California, Oregon, and Washington: Past, Present, and Future. The National Academies Press, Washington, DC.

- Northern Hydrology & Engineering (NHE). 2015a. Humboldt Bay: Sea Level Rise, Hydrodynamic Modeling, and Inundation Vulnerability Mapping. Prepared for the State Coastal Conservancy, and Coastal Ecosystems Institute of Northern California. McKinleyville, CA.
- Patton, J. R., T. B. Williams, J. K. Anderson, and T. Leroy. 2017. Tectonic land level changes and their contribution to sea-level rise, Humboldt Bay region, Northern California: 2017 Final Report. Prepared for U.S. Fish and Wildlife Service Coastal Program. Cascadia GeoSciences, McKinleyville, CA.
- Rhein, M., S.R. Rintoul, S. Aoki, E. Campos, D. Chambers, R.A. Feely, S. Gulev, G.C. Johnson, S.A. Josey, A. Kostianoy, C. Mauritzen, D. Roemmich, L.D. Talley and F. Wang. 2013. Observations: Ocean. In: Climate Change 2013: The Physical Science Basis. Contribution of Working Group I to the Fifth Assessment Report of the Intergovernmental Panel on Climate Change [Stocker, T.F., D. Qin, G.-K. Plattner, M. Tignor, S.K. Allen, J. Boschung, A. Nauels, Y. Xia, V. Bex and P.M. Midgley (eds.)]. Cambridge University Press, Cambridge, United Kingdom and New York, NY, USA.
- Russell, N. and G. Griggs. 2012. Adapting to Sea Level Rise: A Guide to California's Coastal Communities. Prepared for the California Energy Commission Public Interest Environmental Research Program. University of California, Santa Cruz.
- Sweet, W.V., R.E. Kopp, C.P. Weaver, J. Obeysekera, R.M. Horton, E.R. Thieler, and C. Zervas. 2017. Global and Regional Sea Level Rise Scenarios for the United States. NOAA Technical Report NOS CO-OPS 083. NOAA/NOS Center for Operational Oceanographic Products and Services.
- Wolter, K., and M. S. Timlin. 1993. Monitoring ENSO in COADS with a seasonally adjusted principal component index. Proceedings of the 17th Climate Diagnostics Workshop, Norman, OK, NOAA/NMC/CAC, NSSL, Oklahoma Climate Survey, CIMMS and the School of Meteorology, University of Oklahoma: Norman, OK; 52–57.
- Wolter, K., and M. S. Timlin. 1998. Measuring the strength of ENSO events – how does 1997/98 rank? *Weather* ,53, 315–324.
- Wolter, K., and M. S. Timlin. 2011. El Niño/Southern Oscillation behaviour since 1871 as diagnosed in an extended multivariate ENSO index (MEI.ext). *Intl. J. Climatology*, 31(7), 1074–1087.
- Zervas, C., S. 2009. Sea Level Variations of the United States 1854-2006. NOAA National Ocean Service Center for Operational Oceanographic Products and Services. NOAA Technical Report NOS CO-OPS 053. 78pp.
- Zhang Y., J.M. Wallace, and D.S. Battisti. 1997. ENSO-like interdecadal variability: 1900–93. *J Clim* 10:1004–1020.